NMR Solution Structure and Dynamics of the Peptidyl-prolyl cis–trans Isomerase Domain of the Trigger Factor from Mycoplasma genitalium Compared to FK506-binding Protein

9 AUTHORS, INCLUDING:

Tatjana N Parac-Vogt
University of Leuven
144 PUBLICATIONS 2,867 CITATIONS

SEE PROFILE

Klaus M Fiebig
Goethe-Universität Frankfurt am Main
24 PUBLICATIONS 2,954 CITATIONS

SEE PROFILE

JMB

NMR Solution Structure and Dynamics of the Peptidyl-prolyl *cis–trans* Isomerase Domain of the Trigger Factor from *Mycoplasma genitalium* Compared to FK506-binding Protein

Martin Vogtherr[1], Doris M. Jacobs[1], Tatjana N. Parac[1,2]
Marcus Maurer[3], Andreas Pahl[4], Krishna Saxena[1], Heinz Rüterjans[5]
Christian Griesinger[1,6] and Klaus M. Fiebig[1]*

[1]*Institut für Organische Chemie der Universität Frankfurt, Marie-Curie-Str. 11 60439 Frankfurt, Germany*

[2]*K.U. Leuven, Department of Chemistry, Celestijnenlaan 200F, B-3001 Heverlee Belgium*

[3]*Zentaris AG, Weismüllerstr. 45, D-60314 Frankfurt Germany*

[4]*Institut für Pharmakologie und Toxikologie, Universität Erlangen, Erlangen, Germany*

[5]*Institut für Biophysikalische Chemie der Universität Frankfurt, Marie-Curie-Str. 9 60439 Frankfurt, Germany*

[6]*Max-Planck-Institut für Biophysikalische Chemie, Am Faßberg 11, D-37077 Göttingen Germany*

*Corresponding author

We have solved the solution structure of the peptidyl-prolyl *cis–trans* isomerase (PPIase) domain of the trigger factor from *Mycoplasma genitalium* by homo- and heteronuclear NMR spectroscopy. Our results lead to a well-defined structure with a backbone rmsd of 0.23 Å. As predicted, the PPIase domain of the trigger factor adopts the FK506 binding protein (FKBP) fold. Furthermore, our NMR relaxation data indicate that the dynamic behavior of the trigger factor PPIase domain and of FKBP are similar. Structural variations when compared to FKBP exist in the flap region and within the bulges of strand 5 of the β sheet. Although the active-site crevice is similar to that of FKBP, subtle steric variations in this region can explain why FK506 does not bind to the trigger factor. Sequence variability (27% identity) between trigger factor and FKBP results in significant differences in surface charge distribution and the absence of the first strand of the central β sheet. Our data indicate, however, that this strand may be partially structured as "nascent" β strand. This makes the trigger factor PPIase domain the most minimal representative of the FKBP like protein family of PPIases.

© 2002 Elsevier Science Ltd. All rights reserved

Keywords: trigger factor; peptidyl-prolyl *cis–trans* isomerases; NMR structure determination; protein dynamics; FKBP

Introduction

Peptidyl-prolyl *cis–trans* isomerases (PPIases) catalyze the isomerization of peptidyl-prolyl

Abbreviations used: FKBP, FK506 binding protein; GST, glutathione-*S*-transferase; HSQC, heteronuclear single quantum coherence; NOE, nuclear Overhauser effect; NOESY, NOE spectroscopy; PPIase, peptidyl-prolyl *cis–trans* isomerase; ppm, parts per million; rmsd, root-mean-square deviation; RDC, residual dipolar coupling; TF, trigger factor; DMSO, dimethyl sulfoxide.

E-mail address of the corresponding author: kf@org.chemie.uni-frankfurt.de

bonds,[1] for which significant barriers of 80 kJ mol^{-1} between their *cis* and *trans* conformations exist.[2] The slow interconversion between these conformations is often the rate-limiting step in protein folding and justifies enzymes catalyzing this process. By contrast, chaperones, which are another class of proteins assisting protein folding, do so by preventing unwanted tertiary interactions, protein aggregation and misfolding.[3,4]

Three classes of PPIases have been found so far; the cyclophilins, the FK506-binding proteins (FKBPs) and the parvulins. Selected members of each of these three PPIase classes have been
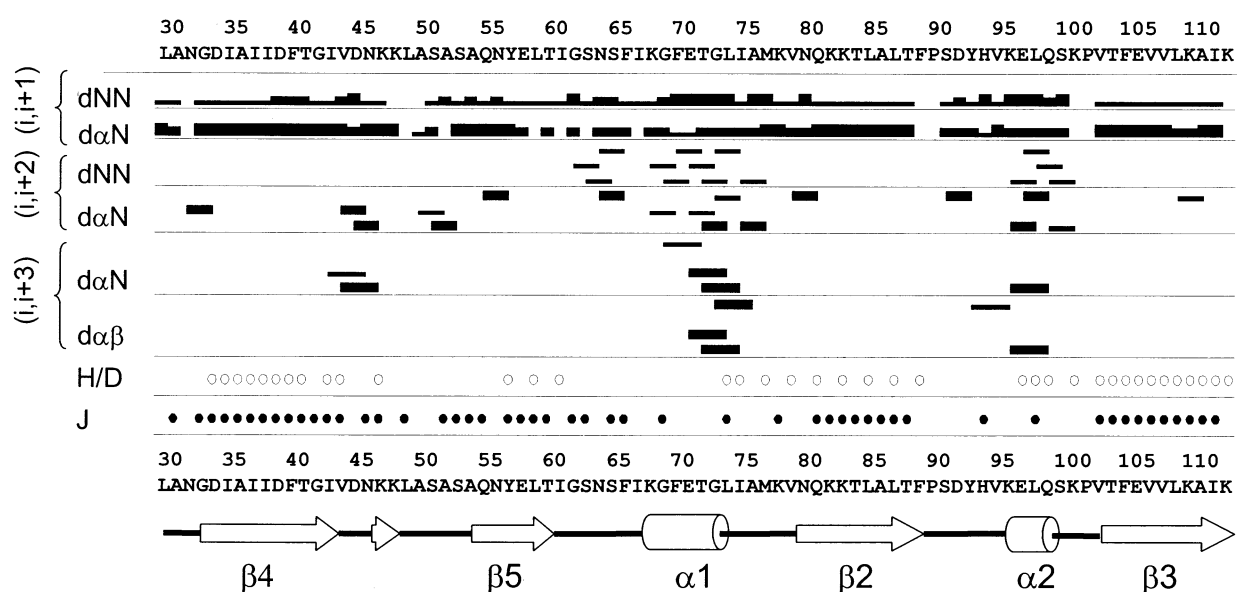
Figure 1. Local NOE and restraint pattern: the sequence of the trigger factor is written at the top. Characteristic NOEs are marked as thin and thick bars according to their intensity. Open circles at the bottom indicate slowly exchanging amide protons. Filled circles at the bottom are drawn for large (>7 Hz) coupling constants. The resulting secondary structure is depicted below.

characterized thoroughly, both functionally and structurally. Cyclophilins and FKBPs are important targets for the immunosuppressive drugs cyclosporin and FK506, respectively. FKBPs and parvulins were found to adopt a similar fold of their PPIase domains, which has been called the FKBP fold,[5] whereas the cyclophilins are not structurally related to the other two groups of proteins.

Another PPIase is the trigger factor (TF). Originally, this 59 kDa protein was found to be involved in *Escherichia coli* membrane transport of secretory export proteins[6] by presumably stabilizing their partially unfolded states.[7] Subsequently, TF was found to associate with the 50 S subunit of the ribosome,[8] and hence thought to be involved in initial folding steps of the nascent peptide chain.[9] Its PPIase activity *in vitro* is very low, but its protein folding activity is the highest among all known PPIases.[10] TF is a modular protein consisting of three domains: an N-terminal ribosome-binding domain,[11] a central PPIase domain, and a C-terminal domain of unknown function.[12] The intact protein has a high affinity toward unfolded polypeptides, even those that do not contain proline residues.

The isolated PPIase domain, however, prefers peptides containing proline.[13] The current view of the role of TF *in vivo* is that of a multifunctional folding catalyst that possesses both PPIase and chaperone activity.[10] Hence coexpression of TF has been reported to increase the yield of correctly folded overexpressed proteins, which would have otherwise been insoluble.[14] Mutants lacking the TF gene compensate for its function by increased expression of DnaK, while a lack of both genes (TF and DnaK) is reported to be lethal.[15,16] This may indicate partially overlapping functions of

both enzymes. Additionally, TF associates with the chaperone GroEL and enhances its ability to bind other proteins.[17] TF also seems to act as a "cold-shock" protein to enhance bacterial viability at low temperature.[18]

Database searches indicate that proteins homologous to TF are present in all sequenced prokaryotic genomes. In the small *Mycoplasma genitalium* genome,[19] TF appears to be the only protein associated with PPIase activity.[20] This emphasizes the important role of TF within the PPIase class, since Mycoplasma bacteria are believed to possess the smallest functional genome of a free-living organism. Furthermore, inhibition of TF might be the basis for antibiotics targeted against these pathogenic organisms.

Here, we will focus on the central domain of the TF, $TF_{151-251}$ (denoted TF_{PPIase} in the text), which was found to be responsible for the PPIase activity of the protein.[21–23] Hydrophobic cluster analysis of the amino acid sequence of TF_{PPIase} revealed a similar pattern of hydrophobic residues for TF_{PPIase} and FKBP.[24] On the basis of the published coordinates of FKBP, several 3D homology models of TF_{PPIase} have been built,[20,24] all of which feature the typical FKBP fold consisting of a five-stranded β-sheet and an α-helix crossing this sheet. Based on the moderate sequence homology between TF_{PPIase} and FKBP (27% identity) conserved residues were predicted to define the active site of TF_{PPIase}. Important differences of the modeled TF_{PPIase} as compared to FKBP were predicted to exist both in the flap region and in strand β5 of the sheet. These regions show the greatest sequence variability when compared to FKBP. Hence, our primary goal was to determine the solution structure of the TF_{PPIase} at atomic resolution and to compare these findings
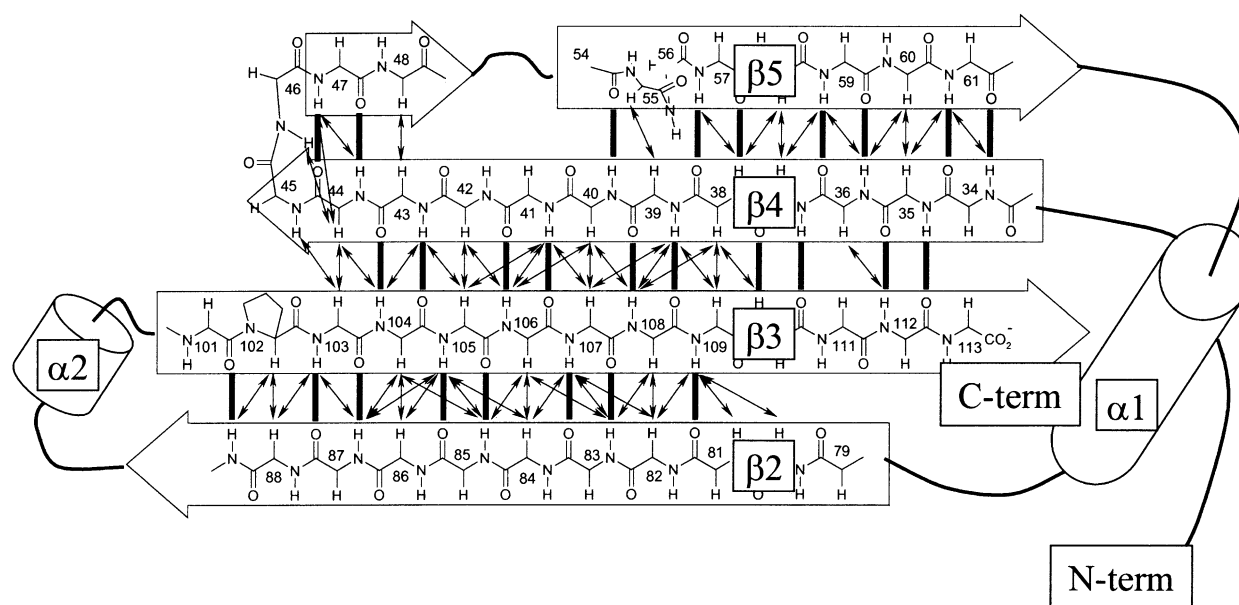
Figure 2. Hydrogen bond and NOE network in the extended β-sheet: from top to bottom, strands 5, 4, 3 and 2 (following the FKBP nomenclature) are indicated. NOEs that define the orientation of the strands are depicted by arrows. Hydrogen bonds identified by slowly exchanging amide protons are shown by bold lines.

with the structure of FKBP and other known PPIases structures. A second objective was to explain why TF, despite its homology to FKBP, does not bind the immunosuppressant drug FK506.

Results and Discussion

Assignment of resonances

For all NMR studies, the 101 amino acid residue PPIase domain of the TF was used. This domain, TF_{PPIase}, begins at Glu13 (Glu151 in the intact trigger factor) and ends with Lys113 (Lys251). The N terminus of TF_{PPIase} was tagged with 12 amino acid residues containing a His$_6$ tag to enable rapid purification. None of the resonances of the His$_6$ tag, with the exception of the Ser immediately preceding Glu13, could be assigned to resonances in the ^{1}H–^{15}N heteronuclear single quantum coherence (HSQC) spectrum. These residues are all presumed to be unstructured (see below).

We have ruled out interactions between the basic histidine tag and the rest of the protein using a construct lacking the His-tag and instead just having a Gly immediately preceding Glu13. This construct, as compared to the His$_6$-tagged protein, has identical chemical shifts in the ^{1}H–^{15}N HSQC spectrum (see Figure 1 of the Supplementary Material) as well as identical nuclear Overhauser effect spectroscopy (NOESY) patterns in the ^{15}N-edited NOESY spectrum.

Backbone and C$^\alpha$ resonances were assigned using a combination of 3D HNCACB[25] and 3D CBCA(CO)NH[26] spectra. For the structured region of TF_{PPIase} all residues, except Ala50, give rise to

distinct amide cross-peaks. The assignment and the extent of assigned resonances have been published.[27]

Secondary structure of the trigger factor

For the N-terminal stretch (Ser12 to Lys29), only intra-residual and sequential NOEs could be detected. This type of NOE signature is typical of unstructured polypeptide chains.[28,29] The well-defined structured region of TF_{PPIase} begins with Leu30. Figure 1 shows local NOEs, HN–H$^\alpha$ coupling constants, H/^{2}H amide backbone exchange rates, and the associated secondary structure elements. For consistency, all secondary structure elements of TF_{PPIase} are named analogously to those of FKBP.

Four strands of the central β-sheet of TF_{PPIase} were identified by slow H/^{2}H amide exchange and/or large $^3J_{HN-H\alpha}$ couplings. This sheet is shown in Figure 2 and is defined by 51 characteristic NOEs (arrows) and 27 slowly exchanging H-bonds (bold lines). Strand β4 consists of residues Gly33 through Asn43. It is separated from strand β5 (Tyr57 to Ile61) by a β-turn (Val44 to Lys47) and a stretch of seven amino acid residues (Lys48 to Gln55) that show some β-sheet character (large $^3J_{HN-H\alpha}$ couplings, strong sequential HN–H$^\alpha$ NOEs and weak sequential HN–HN NOEs) but little H/^{2}H exchange protection. Gly62 to Gly69 do not show any characteristic structural features. For residue Phe70 to Ala76, the NOE pattern, slowly exchanging amide protons and small coupling constants define helix α1. Residues Asn80 to Phe89 and Val103 to Lys113 form β-strands β2 and β3, respectively. Amino acid residues Pro90 to Pro102 separating strands β2

Table 1. Structure calculation statistics of the 12 lowest-energy structures from an ensemble of 200 calculated structures

Average energy values (kcal mol^{-1})	
E total	455 ± 3
E bond	9.7 ± 0.5
E angle	126 ± 2
E improper	35.4 ± 1
E vdW	91 ± 3
E NOE	35 ± 3
E dihedral	0.4 ± 0.05
E J coup	78 ± 2
E vector-angle	79 ± 2
RMS deviation from idealized covalent geometry	
Bond length (Å)	0.0025 ± 0.00006
Angles (deg)	0.538 ± 0.005
Impropers (deg)	0.55 ± 0.008
Dihedral angles (deg)	31 ± 0.6
RMS deviations from experimental data	
Distance restraints (Å)	0.0210 ± 0.0008
Dihedral restraints (deg)	0.21 ± 0.01
$^3J_{HN-HA}$ (Hz)	1.06 ± 0.02
Coordinate rmsd deviation (Å) (residues 30–112)	
Backbone atoms	0.234
All heavy atoms	0.725
Analysis of Ramachandran plot of structured region of TF$_{PPIase}$ (residues 29–113), number of residues in the ensemble of 12 structures	
Residues in most favored regions (%)	574 (62.9)
Residues in additional allowed regions (%)	296 (32.5)
Residues in generously allowed regions (%)	30 (3.3)
Residues in disallowed regions (%)	12 (1.3)
Analysis of residual dipolar couplings	
Q-value	0.25–0.26
Correlation coefficient	0.97

These 12 structures were submitted to the Protein Data Bank, database entry 1HXV. Statistics were generated from CNS and PROCHECK output.

and β3 correspond to the "flap" region in FKBP and consist of a loop-like structure followed by a short 3$_{10}$ helix (α2).

Tertiary structure

Using standard molecular dynamics protocols (see Materials and Methods), an ensemble of 200 structures was calculated with the following NMR data: 959 interresidual NOEs, 35 hydrogen bonds, 72 $^3J_{HN-H}$α coupling constants, 68 dihedral angle restraints and 2628 dipole–dipole projection restraints[30] derived from 68 amide dipolar couplings (Table 1). Figure 3 shows the distribution of NOEs and the resulting backbone rmsd as a function of sequence position. The backbone rmsd clearly anticorrelates with the number of NOE restraints per amino acid residue, identifying several loops with reduced constraint density. On average, 11 interresidual NOEs per residue could be extracted from the NMR data. These restraints define a tight ensemble of structures, for which the 12 lowest-energy structures (of 200 calculated) display a backbone rmsd of 0.23 Å and an rmsd of 0.72 Å for all heavy atoms. No NOE violations

over 0.5 Å and maximally one NOE violation between 0.2 and 0.5 Å were found. Statistics for this ensemble, as calculated by CNS,[31] PROCHECK[32] and DipoCoup,[33] are compiled in Table 1. Figure 4 shows a stereo drawing of these 12 lowest-energy structures, fit for minimal backbone rmsd of the region Lys29-Lys113.

The TF$_{PPIase}$ structure was additionally restrained using residual dipolar couplings (RDCs). The same data set without RDCs leads to a distinctly higher backbone rmsd of 0.3 Å *versus* 0.23 Å including RDCs. Concomitantly, the RDC Q value[34] drops from 0.5 without RDCs to 0.28 with RDCs, hence the agreement of the structure with the measured couplings is greatly improved. Especially the flap region (residues Pro90 to Pro102) becomes much better defined with the use of RDCs, balancing the relative scarceness of NOEs in this region. It should be stressed that the NOE and the RDC data sets do not contradict each other, which is reflected by unchanged NOE energies when RDC-restraints are used in the simulation.

NMR data indicate a βI′ turn between strands β4 and β5, which implies that Asp46 is the only residue that is found in a disfavored region of the Ramachandran plot ($\Phi = 80°$; $\Psi = -40°$). To support the positive Φ angle, we have analyzed the doublet splitting arising from the HN–Hα coupling, which can be resolved by an $^1H-^{15}N$ transverse relaxation optimized spectroscopy (TROSY) experiment.[35] The relative intensities in this doublet depend on Φ due to dipole–dipole cross-correlated relaxation.[36] For Asp46 the high-field component of the doublet is the stronger, consistent with a positive Φ angle.

The trigger factor adopts the FKBP fold

Figure 5 compares an averaged structure of TF$_{PPIase}$ derived from the 12 lowest-energy structures to the structure of uncomplexed FKBP.[37] Clearly, the overall fold of the TF$_{PPIase}$ is similar to that of FKBP. This had been predicted by homology modeling.[20,24] It is therefore reassuring that the main structural features of this model agree well with our experimental structural findings. To ease comparisons between human FKBP12, the different trigger factor variants discussed (*M. genitalium* and *E. coli*), and human Pin1, Figure 6 shows a sequence alignment and structure comparison between these proteins.

The main structural element of FKBP[38–40] as well as of TF$_{PPIase}$ is the extended multi-stranded anti-parallel β sheet with its distinctive topological connectivity. Surprisingly the first strand (1) of this sheet is absent from our structure. Residues of this N-terminal segment of TF$_{PPIase}$ appear to be unstructured, on the basis of the absence of tertiary NOEs and the presence of fast-exchanging amide protons. Also, for strand β2, there is no evidence for an additional strand (inter-strand NOEs or slow exchange of the relevant amide protons).
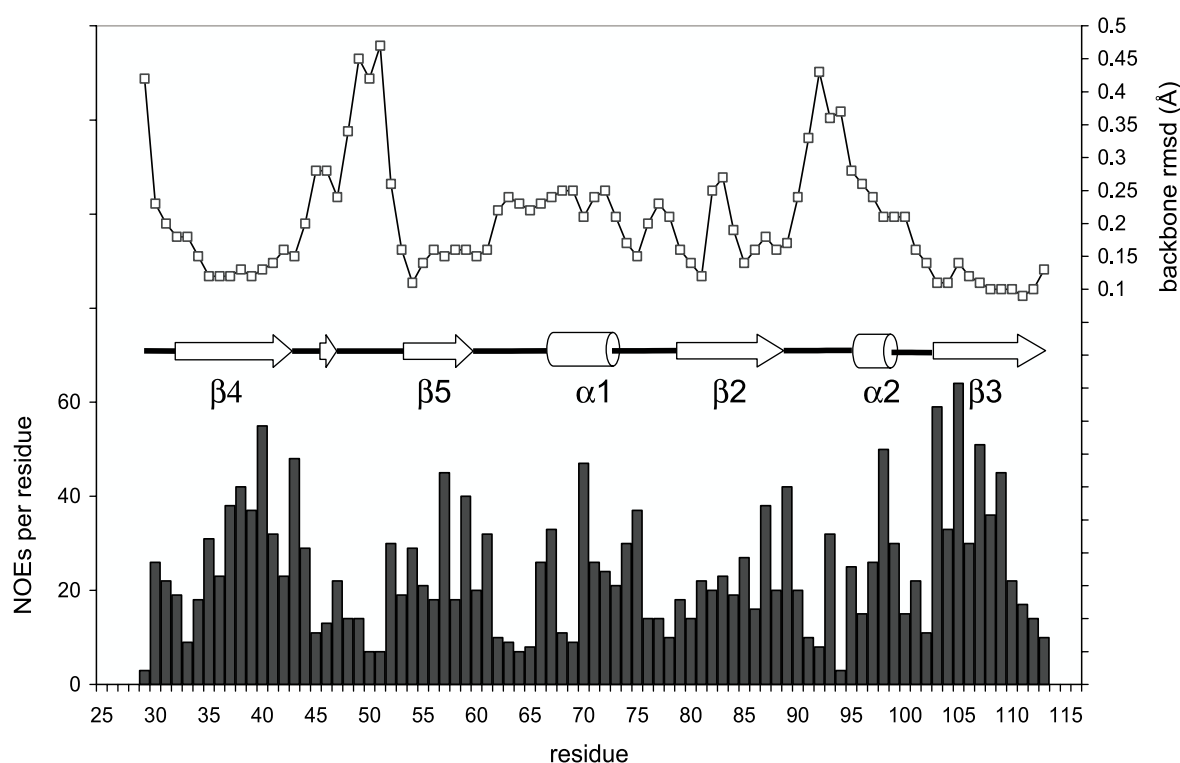
Figure 3. NOE data and rmsd statistics of the folded PPIase domain of the trigger factor (residues 29–113). The number of interresidual NOEs per residue is displayed as vertical black bars. On average, more than 11 interresidual NOEs per residue could be observed. Above the NOE statistics the per-residue backbone rmsd of the 12 lowest-energy structures obtained from an ensemble of 200 calculated structures is shown. The overall backbone rmsd in the resulting structure (omitting the N- and C-terminal lysine residues) is 0.23 Å.

The lack of this β1 strand in TF_{PPIase} circumvents the +3, +1, −3, −1 sheet topology[41] that is distinctive for the FKBP fold and which would involve an unfavorable strand crossing near residue Lys29. Although the N terminus of TF_{PPIase} may be structured in the full-length protein due to domain–domain interactions, testing this hypothesis is not within the scope of the current study. All we can say is that this extra strand does not contribute much to the integrity of the central

sheet of TF_{PPIase}. This is consistent with the structures of the homologous proteins hPar14[5] or hPin1[42] showing a similar absence of the first β strand.

To verify that the N-terminal β1 strand is not structurally relevant, a shortened TF_{PPIase} fragment containing only the folded part of the TF_{PPIase} domain, i.e. residues 168–251 of the full-length TF (denoted $TF_{168-251}$), was expressed. Comparing $^1H-^{15}N$ HSQC spectra of $TF_{168-251}$ and TF_{PPIase}, we

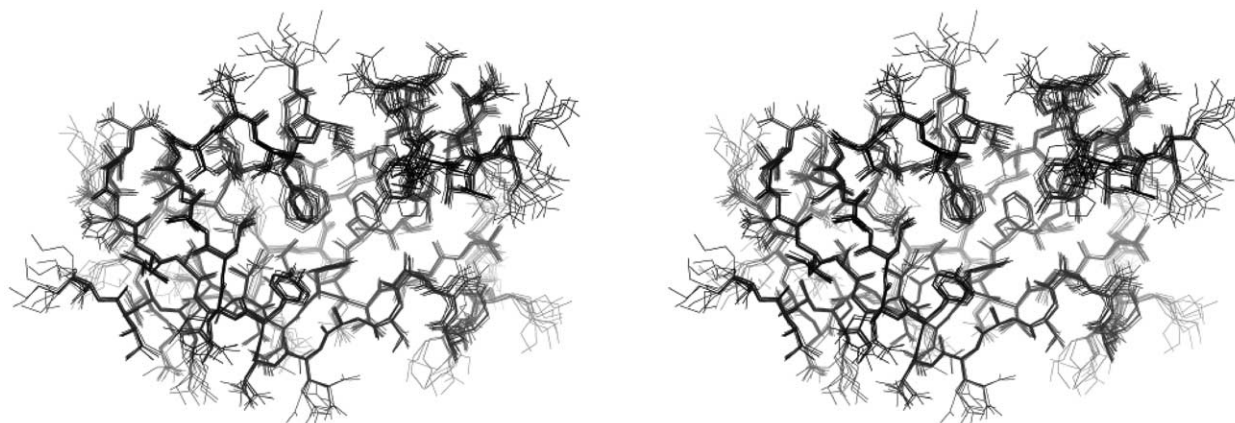**Figure 4**. Stereo drawing of the superposition of the 12 lowest-energy TF_{PPIase} structures. Only the folded parts of the TF_{PPIase} structure (residues 29–113) are shown. The orientation of the structure is the same as in Figure 5, with the active-site cleft towards the viewer and the extended β-sheet at the bottom.
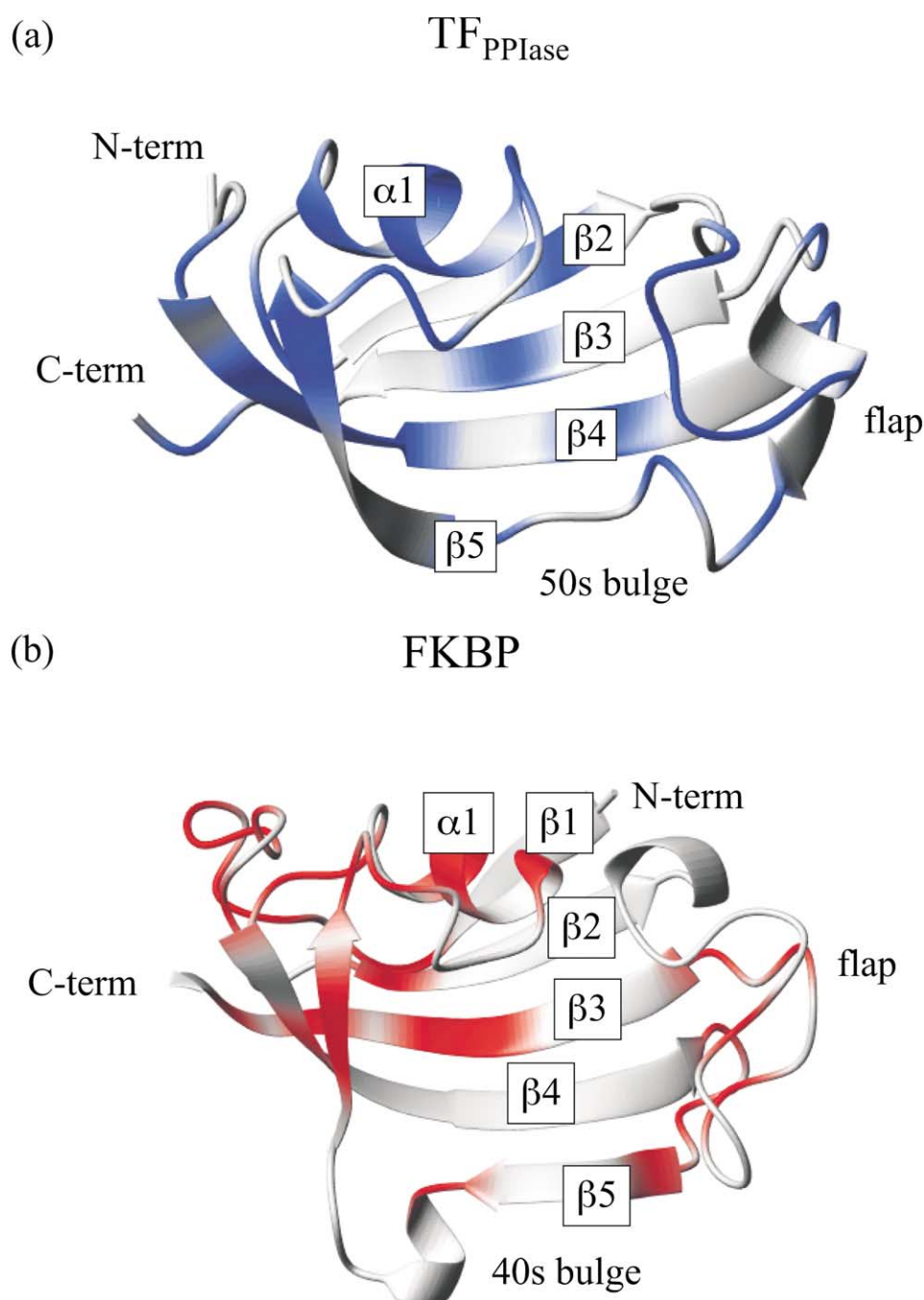
(a)   TF$_{PPIase}$

(b)   FKBP

Figure 5. Structural and dynamic comparison of (a) TF$_{PPIase}$ and (b) human FKBP-12. All secondary structure elements, including the flap and the bulge region are labeled. These proteins are very similar with respect to their overall folding topology. The main differences between the two structures are in the 40s bulge of strand β5, in the flap region and in the absence of the β1 strand. Both proteins are color-coded to represent the relaxation data. Colored regions mark residues that are flexible, and white areas those that are more rigid.

found that most of the protein amide resonances are unaffected by the deletion (Figure 2 of the Supplementary Material). Thus, the global fold of the shortened and the full-length variant is identical. Surprisingly, as seen in Figure 7, the only peaks that have shifted slightly, but significantly (0.1 ppm in both dimensions) in the ^{1}H–^{15}N HSQC spectrum of TF$_{168-251}$ (see Figure 2 of the Supplementary Material) cluster in a well-defined region comprising the strand β2 and the solvent-exposed part of helix α1. This is exactly where the missing β1 strand would be expected. Hence, we believe that the N terminus, despite being essentially unstructured, does interact with the fully structured strand β2 and is best described by a partially structured or "nascent" β1 strand.
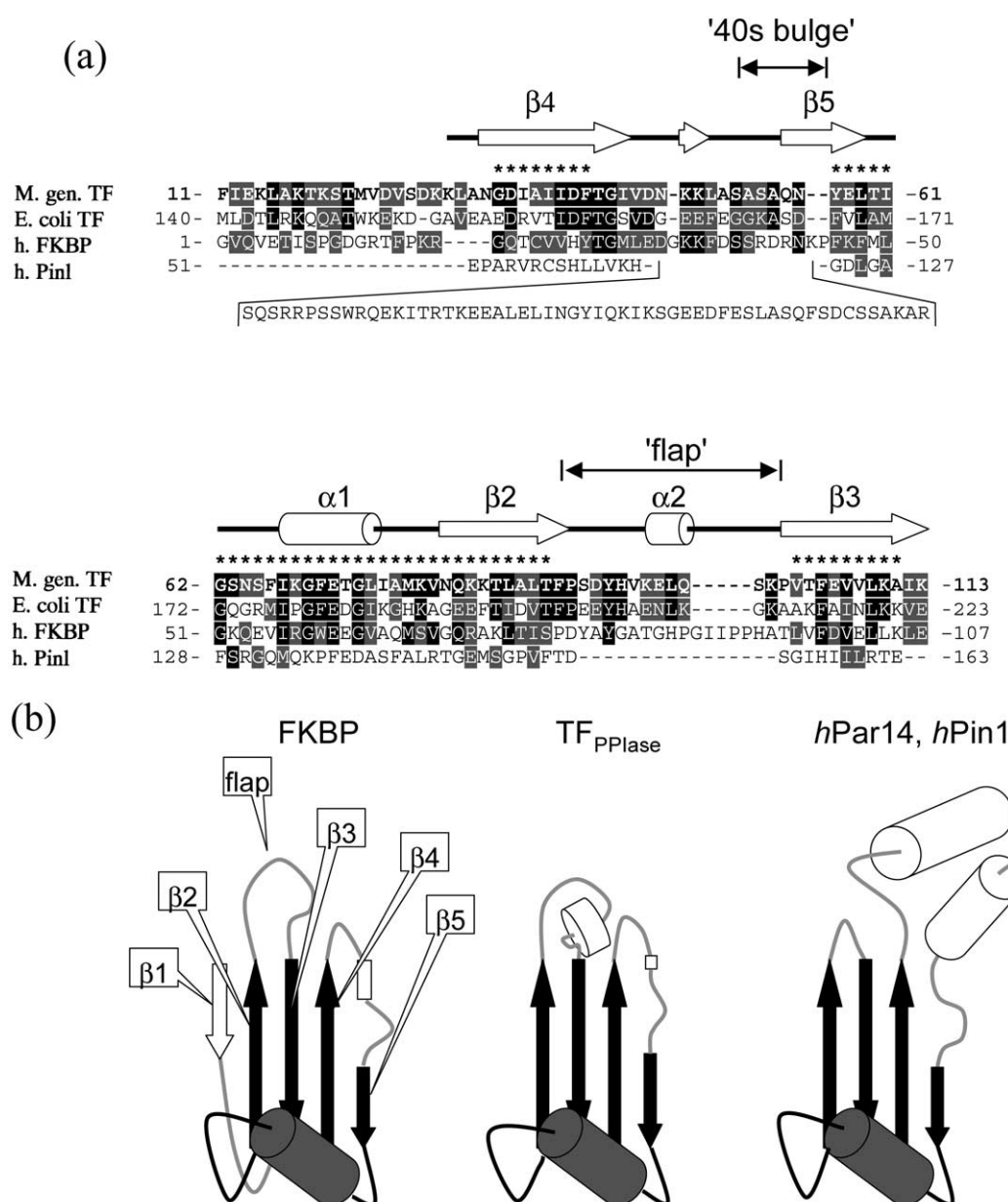
Figure 6. (a) Alignment of the sequence of TF$_{PPIase}$ from *M. genitalium* with *E. coli* TF$_{PPIase}$, human FKBP and human Pin1. The consensus secondary structure is indicated. The sequences used for superposition of the structures are marked with an asterisk (*). Superposition using marked residues results in an rmsd of 1.3 Å for FKBP and 2.4 Å for Pin1. There is 27% sequence identity between TF$_{PPIase}$ and FKBP but only a few randomly scattered amino acid residues are conserved between TF$_{PPIase}$ and Pin1. (b) Comparison of FKBP to other PPIases (adapted from Sekerina *et al.*[5]): FKBP, parvulin, PIN1 and TF share a common fold consisting of the four-stranded β-sheet and of helix α1 (depicted in black). The differences shown in gray are found within the flap region, within the bulges of strand β5 and in the presence of the β1 strand.

Structural similarity and diversity across the FKBP fold

The term FKBP fold has been suggested when comparing the fold of four PPIases of known structure (FKBP12, *h*Pin1, *h*Par4 and GreA tcf).[5] Figure 6 compares TF$_{PPIase}$ with other members of this family. The conserved moiety of this fold (black) comprises the loop-helix-loop motif, including helix 1 and four strands of the five-stranded β sheet. On the other hand, a high level of diversity among these structures is found within the flap region, within the N-terminal half of strand β5, the "40s bulge" in FKBP, and in the presence or absence of the N-terminal β-strand (β1).

To estimate structural similarities between TF$_{PPIase}$ and FKBP, we have superimposed the two structures, using the alignment shown in Figure 6. The agreement of the complete structures (aligning analogous amino acid residues in both proteins) is poor, resulting in a backbone rmsd of 3.7 Å. It
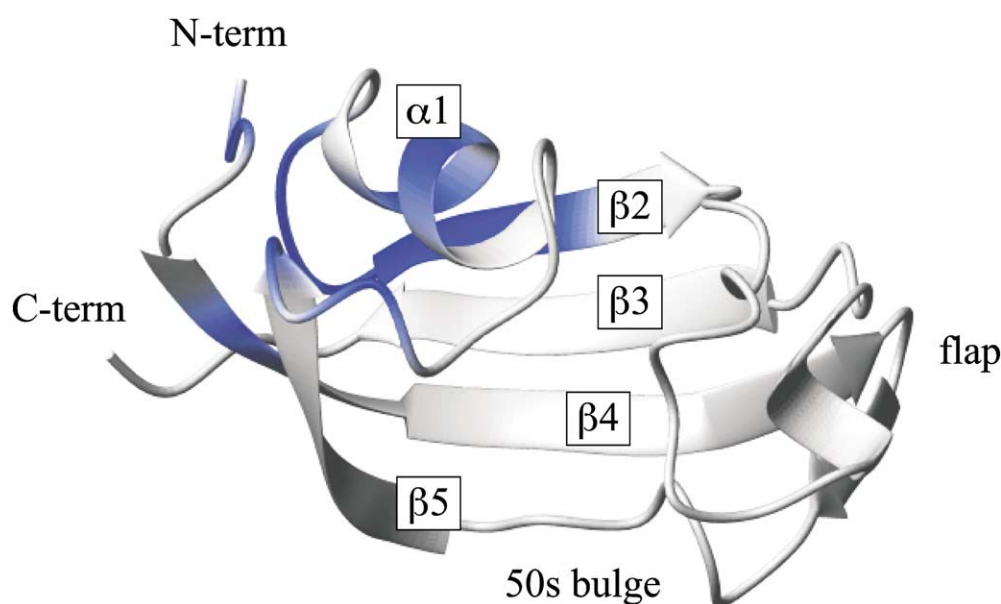
Figure 7. Mapping of chemical shift differences between the complete TF$_{PPIase}$ domain and the deletion mutant TF$_{168-251}$ lacking 17 N-terminal residues. Amino acid residues are color-coded depending on the magnitude of the chemical shift differences between both proteins. These shifts indicate weak interactions of the N terminus (corresponding to the β1 strand in FKBP) with the β2 strand and helix α1, forming a nascent β1 strand.

drops to 1.5 Å when the "bulge" (residues 50–56) and the flap (residues 88–101) are omitted. Obviously, these two regions account for most of the sequential and structural variations between the two proteins. The backbone rmsd drops further to 1.3 Å when only the amino acid residues marked by an asterisk in the alignment are used for fitting.

These residues correspond to the black areas in the secondary structure topology drawing in Figure 6. The resulting superposition of FKBP and TF$_{PPIase}$ shown in Figure 8 illustrates the fact that the main deviations between the two backbone geometries are in the flap and the bulge regions.
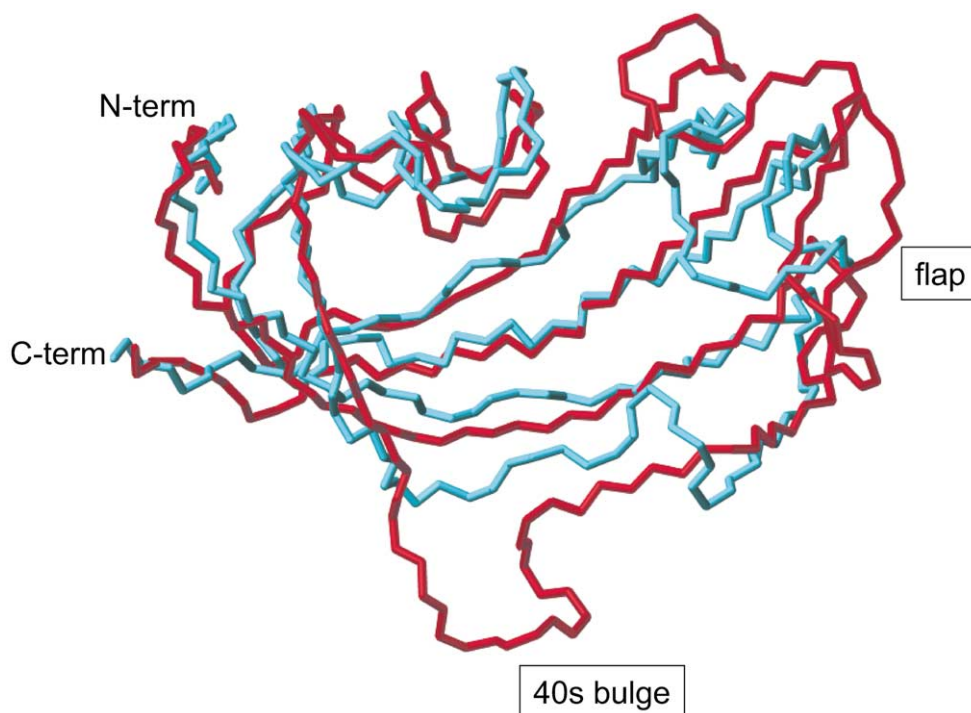

Figure 8. Superposition of the lowest-energy solution structure of TF$_{PPIase}$ (blue) and the X-ray structure of FKBP (red). For FKBP the N terminus (residues 1–15) is omitted for clarity. Coordinates for FKBP were taken from the FKBP–FK506 complex, PDB entry 1FKF. The structures were superimposed using residues marked by asterisks in Figure 6, resulting in an rmsd value of 1.3 Å.

The sequence identity (27%) of the structurally aligned sequences of TF_{PPIase} and FKBP is higher than between TF_{PPIase} and other members of the PPIase family (virtually no sequence identity). Pin1 and parvulin both lack the flap, and both feature an extended α-helical insert. While TF_{PPIase} and Pin1 can be aligned structurally with a slightly worse rmsd (2.4 Å), using analogous amino acid residues as for the TF_{PPIase}-FKBP superposition, these structural alignments do not correspond to homologies in the sequence (Figure 6).

Assuming that conserved structural features indicate common function and structural variability encodes differing function, it is intriguing to postulate different functional roles for conserved and variable regions. For PPIases, the common function is peptidyl-prolyl *cis–trans* isomerase activity. Most of the residues that comprise the proline binding pocket (excluding only Tyr82 for FKBP or Tyr93 for TF_{PPIase}) are located within the structure-conserved parts of these proteins.[38,40] Non-conserved structural features may encode peptide substrate specificity[43] or may facilitate specific interactions with other domains (TF) or even proteins (FKBP).

The flap and the 40s bulge region are different from FKBP

As seen in Figure 8, the major differences between FKBP and TF_{PPIase} are found within the flap region connecting strands β2 and β3 and in the 40s bulge that interrupts strand β5. In TF_{PPIase}, the flap (Thr88 to Pro102) is shortened by six amino acid residues when compared to FKBP (Thr76 to Ser96). In FKBP, this region has no secondary structure elements, while in TF_{PPIase} a single turn of a 3_{10}-helix is found. Despite the different backbone geometries, the resulting van der Waals surface shape of the flap is strikingly similar for these proteins.

The 40s bulge FKBP and its TF_{PPIase} counterpart, the 50s bulge, disrupt strand β5 of the sheet. In FKBP, this bulge spans Ser39 to Phe46. In TF_{PPIase}, this bulge is shortened by three amino acid residues and shifted towards the N terminus (Leu49 to Ser53). In TF_{PPIase} only a two residue kink at the exact position of FKBP's bulge (Ala54 to Tyr57) remains. In FKBP, the 40s bulge is a large patch protruding from the protein, whereas for TF_{PPIase} this region essentially has regular β-sheet character. Hence, the van der Waals surfaces of the two proteins differ significantly at this location.

Strand β5 of FKBP contains the conserved Asp37, which was found to be important for binding of FK506 and rapamycin (38–40) and the recognition of a substrate peptide,[44,45] with O^{δ} of Asp37 serving as hydrogen bond acceptor. The superposition of the TF_{PPIase} and FKBP structures (Figure 8) places the backbone carbonyl oxygen atom of Ser51 in TF_{PPIase} into almost exactly the same position as the aspartate side-chain oxygen atom in FKBP. Hence, side-chain mutations of Ser51 in *M. genitalium* TF_{PPIase} or Glu180 in *E. coli* TF, which correspond to Asp37 of FKBP, will be unlikely to affect the PPIase activity, as has been observed for *E. coli* TF mutants.[46]

Both the 40s bulge and the flap region modulate the protein surface around the PPIase active site. These regions show a high degree of variability across the whole family of PPIases of the FKBP superfold.[5,38–40,42] On the other hand, the variations between FKBPs originating from different species are rather low.[47] Hence, these regions can be regarded as functional fingerprints. They may modulate specificity towards prolyl bonds in various sequence contexts or enable interactions with other proteins.

In addition to shape, the surface charge distribution may determine substrate specificity. Hence, we have calculated the electrostatic surface potential of both proteins, TF_{PPIase} and FKBP. Both proteins feature a hydrophobic active-site cleft, framed by the flap region, which is dominated by basic histidine side-chains and the 40s bulge, which differs in charge distribution between the two proteins (see Figure 2 of the Supplementary Material). For FKBP, a basic patch of Arg42, Lys44, and Lys47 dominates the 40s bulge. The same region in TF_{PPIase}, a regular β-sheet region, is distinctly acidic in character due to the presence of Glu58 and Asp34.

Peptide substrates can interact with the flap region and the 40s bulge. If peptide substrate recognition is driven by electrostatic interactions with the acidic patch, then basic sequences would be preferred over acidic sequences. This effect has been observed experimentally.[43]

The importance of shape and charge complementarities in protein–protein interactions is well documented for the FKBP–FK506 complex, which forms a tertiary complex with calcineurin.[48] Indeed, a lot of critical interactions of the A and B chain of calcineurin involve binding to the 40s bulge and to the flap region. Furthermore, the loop of calcineurin A that packs tightly against the 40s bulge of FKBP is rich in acidic side-chains, being complementary to the basic 40s bulge. For TF_{PPIase}, probably the most relevant protein–protein (or domain–domain) interaction is the tertiary organization of the complete three-domain TF protein, for which few if any data are available. It is only known that the full-length TF interacts with GroEL,[17] but it is not clear which domain is responsible for this interaction.

The trigger factor does not bind FK506 due to steric hindrance

One of the first differences observed between FKBP and TF_{PPIase} is that FK506 is a potent inhibitor of FKBP's PPIase activity, while TF_{PPIase} remains unaffected by FK506.[8] We have therefore interpreted this difference from a structural point of view.

Table 2. Equivalent residues or functional groups that are involved in binding of FK506 in FKBP and of the substrate in both proteins

FKBP		TF$_{PPIase}$	
A. *Hydrophobic contacts*			
Tyr26		Phe40	
Phe46		Tyr57	
Phe99		Phe105	
Ile56		Ile67	
Trp59		Phe70	
B. *Hydrogen bonds*			
Ile56	HN	Ile67	HN
Asp37	COO⁻ (side-chain)	Ser51	CO (backbone)
Tyr82	OH	Tyr93	OH
Glu54	CO	Ser65	CO

In the past, the question of whether FK506 affects TF PPIase activity has been somewhat controversial. Although convincing data exist that *E. coli* TF does not bind FK506,[8] weak inhibition of PPIase activity by FK506 has been observed for *Bacillus subtilis* TF.[23] We have reinvestigated the binding of FK506 to *M. genitalium* TF$_{PPIase}$ using NMR techniques that provide a generic binding assay independent of any biochemical assay and can detect even weak binding. Saturation transfer difference spectra[49] of TF$_{PPIase}$ plus FK506 show no signals. Also, upon addition of FK506, no amide resonances were shifted in the ^{1}H–^{15}N HSQC spectrum of TF$_{PPIase}$. Furthermore, FK506 did not compete with dimethyl sulfoxide (DMSO) which binds weakly ($K_D = 200$ mM) to the active site of TF$_{PPIase}$. Hence, there is strong evidence that FK506 does not bind the TF$_{PPIase}$ domain of *M. genitalium*. As described below, our structural data strongly support these findings.

The crystal structure of the FKBP–FK506 complex[38,40] identifies residues involved in the interaction of FKBP with FK506. Many of these residues are conserved if not identical in FKBP and TF$_{PPIase}$ (Table 2 and Figure 9). Two aromatic side-chains are swapped (Tyr26/Phe46 in FKBP *versus* Phe40/Tyr57 in TF$_{PPIase}$) and the conserved Trp59 is replaced by a phenylalanine residue both in *M. genitalium* and *E. coli* TF.

Whether the conserved Trp59 in FKBP is an essential mediator for FK506-binding has been tested for *E. coli* TF by creating a more "FKBP-like" TF mutant W59F.[46] Unfortunately, this mutation led to a protein that was highly unstable.
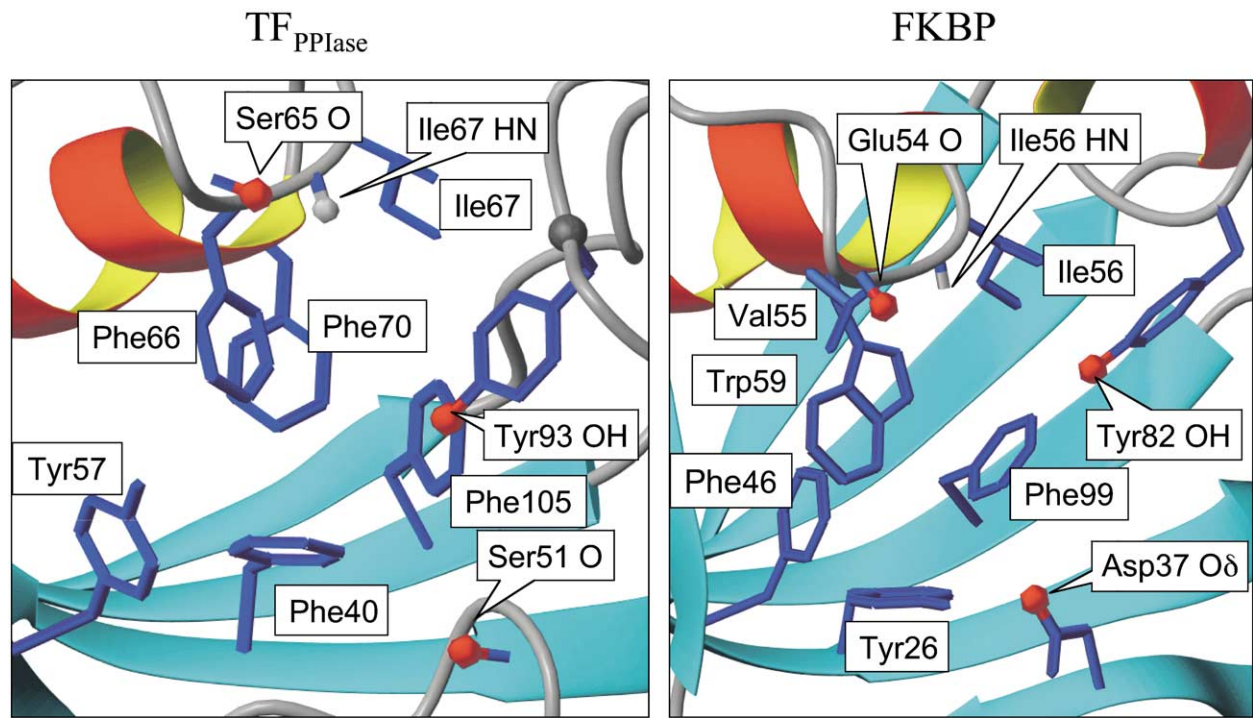

Figure 9. Ribbon representations of the putative active sites of TF$_{PPIase}$ (left) and FKBP (right). Conserved side-chains and functional groups that were found to be important for FK506 binding to FKBP and their equivalents in TF$_{PPIase}$ are displayed as stick representations in both structures.
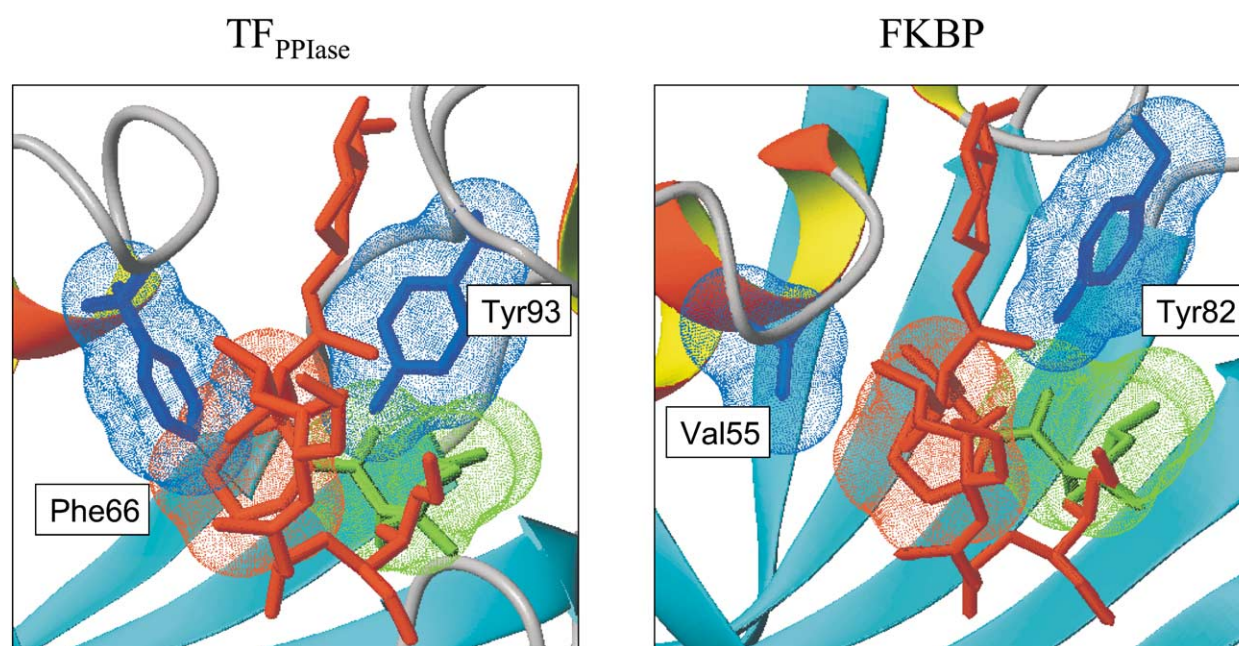
Figure 10. Model of the hypothetical TF$_{PPIase}$−FK506 complex (left) and comparison with the actual FKBP−FK506 complex (right). The hypothetical TF$_{PPIase}$−FK506 complex is based upon the same superposition of TF$_{PPIase}$ and FKBP as in Figure 8. Regions of FK506 and of TF$_{PPIase}$ experiencing steric clashes are indicated by their dotted van der Waals surfaces. Blue, residues Phe66 and Tyr93 (TF$_{PPIase}$) that interfere with the binding in TF$_{PPIase}$ and the corresponding Val55 and Tyr82 of FKBP. Regions of FK506 in conflict with the binding to TF$_{PPIase}$ are displayed in red and green, respectively, and are colored according to Scheme 1.

Trp59 in FKBP has hydrophobic contacts with two valine residues (Val24 and Val63), whereas their bulkier counterparts in *E. coli* or *M. genitalium* TF$_{PPIase}$, leucine and isoleucine, leave insufficient space for a Phe-Trp replacement. Likewise a F70H mutant was not stable, since a polar side-chain is not compatible with the hydrophobic environment of Phe70.

Another difference is Asp37, which does not have a structural analog, since the backbone structure is altered significantly in this region. However, the H-bond acceptor O$^\gamma$ of Asp37 is replaced adequately by the backbone oxygen atom of Ser51, as discussed above. Since the 3D arrangement of all other critical residues is essentially the same for both proteins, these subtle differences alone can hardly explain why FK506 does not bind to TF$_{PPIase}$.

Our conclusion that TF$_{PPIase}$−FK506 binding is prohibited originates from the analysis of a hypothetical TF$_{PPIase}$−FK506 complex, which shows that binding of FK506 is sterically highly unfavorable. This hypothetical complex is modeled utilizing the superposition of TF$_{PPIase}$ and the FKBP−FK506 complex (see Figure 8). Figure 10 shows a detailed view of this hypothetical TF$_{PPIase}$−FK506 complex compared to the experimental FKBP−FK506 complex. Due to differences in backbone geometry of the flap region, the conserved Tyr93 is located at a position that is shifted by 1−2 Å into the cleft when compared to its position in FKBP, leading to steric overlap with the FK506 pyranose ring (color-coded green in Figure 10 and

Scheme 1). Furthermore, Val55 of FKBP, which forms part of the hydrophobic pipecolyl binding pocket, is replaced by the much bulkier Phe66 in TF$_{PPIase}$. In TF$_{PPIase}$ Phe66 interferes with binding of the FK506 pipecolyl ring (color-coded red in Figure 10 and Scheme 1).

Since these arguments are based on a hypothetical model, they cannot account for conformational flexibility of the aromatic side-chains, which could give way to accommodate FK506. They also cannot account for motions of Phe66 and Tyr93 relative to each other, as might be expected from our relaxation analysis (see below). Nevertheless our view is that two main structural factors prevent FK506
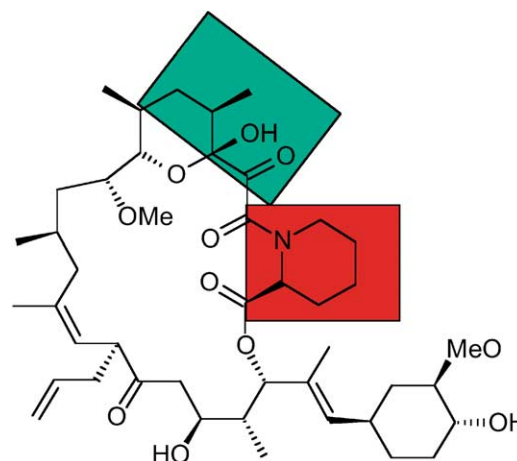
Scheme 1.

binding to TF$_{PPIase}$: (1) the altered backbone geometry of the highly variable flap region; and (2) the side-chain replacement Phe to Val in a conserved loop. Taken together, these two aspects lead to a much narrower hydrophobic binding cleft and make binding of the large FK506 molecule highly unfavorable.

The structure of the active site is conserved between TF and FKBP

The fold of the extended sheets and the loop-helix α1-loop motif is strikingly similar in TF$_{PPIase}$ and FKBP. Since this structural homology is found in other PPIases, it appears to be linked to the PPIase activity directly.

Currently, the definition of the PPIase active site remains speculative, since a structure of a protein–substrate complex of TF$_{PPIase}$ or FKBP has not been published. Crystallization of such a complex is difficult due to the low (millimolar) affinities of TF and FKBP towards their target peptides. For the interaction of TF$_{PPIase}$ with a standard peptide, Suc-Ala-Ala-Pro-Phe-pNO₂, NMR titration studies yield a K_d of 0.1 mM (data not shown), which compares well with the K_M of 0.52 mM of the same peptide binding to FKBP.[50] Cyclophilins and parvulins have a much higher affinity towards their substrates and thus have been cocrystallized with a minimal substrate, Ala-Pro.

The only structural basis of FKBP's PPIase activity can be inferred by using the FK506–FKBP complex as a model, where the pipecolyl moiety of FK506 is assumed to mimic the peptidyl-prolyl bond.[38,40] With this approach, two enzyme–substrate complexes for FKBP were modeled to rationalize enzyme–substrate recognition.[44,45] These studies have identified several residues that appear to be involved in protein–substrate interactions. These residues and their TF$_{PPIase}$ counterparts are shown in Figure 9 and listed in Table 2.

FKBP's active-site cleft is defined by the aromatic side-chains of Tyr26, Phe46, Phe99, and Trp59. This cleft can accommodate the hydrophobic pipecoline ring of FK506, which is assumed to mimic the proline ring. FK506 binding to FKBP changes its conformation around the pipecoline ring from *cis* in the free state to *trans* in the complex. The carbonyl oxygen atom is hydrogen bonded to the amide group of the conserved Ile56 of FKBP (Ile67 for TF$_{PPIase}$). In FKBP, this amide has a greatly enhanced hydrogen bond donor potential, leading to the formation of specific hydrogen bonds even to small molecules like DMSO.[37,51] For TF$_{PPIase}$, we find large shifts for the corresponding Ile67 amide resonances upon addition of the peptide substrate or DMSO. The mode of binding to the peptide substrate can therefore be assumed to be similar for both proteins.

Other hydrogen bonds involving the backbone of Glu54 and side-chains of Tyr82 and Asp37 were considered important for enzyme–substrate recognition (Table 2). In TF$_{PPIase}$, the relative 3D

arrangement of these groups is essentially the same (see Figure 9). The only differences are the narrowing of the hydrophobic cleft by the aromatic side-chain of Phe66, and a repositioning of one hydrogen bond donor, the tyrosine hydroxy group, by 1–2 Å (see above).

Since the TF$_{PPIase}$ substrate-binding site is narrower and thus more restrictive than that in FKBP, the TF$_{PPIase}$ domain may be more selective with respect to its substrates. This is confirmed by experimental data concerning the stereoselectivity of both proteins.[52] While FKBP also catalyzes isomerization in peptides that contain a D-proline residue at the critical position, this is not the case for TF$_{PPIase}$. For these D-Pro-containing peptides, the kinetic data yield a much larger Michaelis–Menten constant, indicating that these substrates are bound by TF$_{PPIase}$ less tightly than by FKBP.

Peptide substrate variability has been addressed in several additional studies, which have explored the nature of the residue preceding the prolyl bond (the P1 site), both for FKBP and for TF.[8,23,46,53] Both proteins show the same preference for bulky, hydrophobic side-chains and no tolerance for negatively charged side-chains. The preference for a bulky side-chain (as judged by relative catalytic efficiencies) is higher for TF$_{PPIase}$ than for FKBP, which apparently contradicts the narrower binding-cleft hypothesis. However, the P1 side-chain is located at some distance from the proline-binding site where the narrowing occurs. Nevertheless, detailed knowledge of the peptide's binding mode will be necessary for a more extensive characterization of substrate binding.

TF$_{PPIase}$ and FKBP show similar dynamic behavior

The dynamic properties of TF$_{PPIase}$ were probed by measuring ^{15}N relaxation parameters. Figure 11 shows longitudinal (R_1) and transversal (R_2) relaxation rates as well as {^{1}H}–^{15}N heteronuclear NOE values for a total of 91 backbone amide protons (89% of all possible). No data are presented for residues for which assignments are missing (residues 14, 15, 17, 19, 20, 50, and 51) or for those with significant overlap in the ^{1}H–^{15}N-HSQC spectrum (residues 25 and 81). Excluding the N-terminal 18 residues, the average {^{1}H}–^{15}N NOE value of 0.80 ($\pm$0.03) indicates that most regions of TF$_{PPIase}$ are relatively rigid, which is consistent with the narrow distribution of conformers in the calculated ensemble. Within the structured region, only Ile67 exhibits internal motion on the nanosecond to picosecond time-scale, which may be of importance for its role as hydrogen bond donor. Some residues (residues 33, 34, 37, 63, 64, 70, and 110) show {^{1}H}–^{15}N NOE values above the theoretical maximum of 0.834, which may be due to chemical exchange with the solvent, provided the errors of these values are not underestimated.[54]

The N-terminal 18 residues are flexible in solution, as evidenced by {^{1}H}–^{15}N NOE values
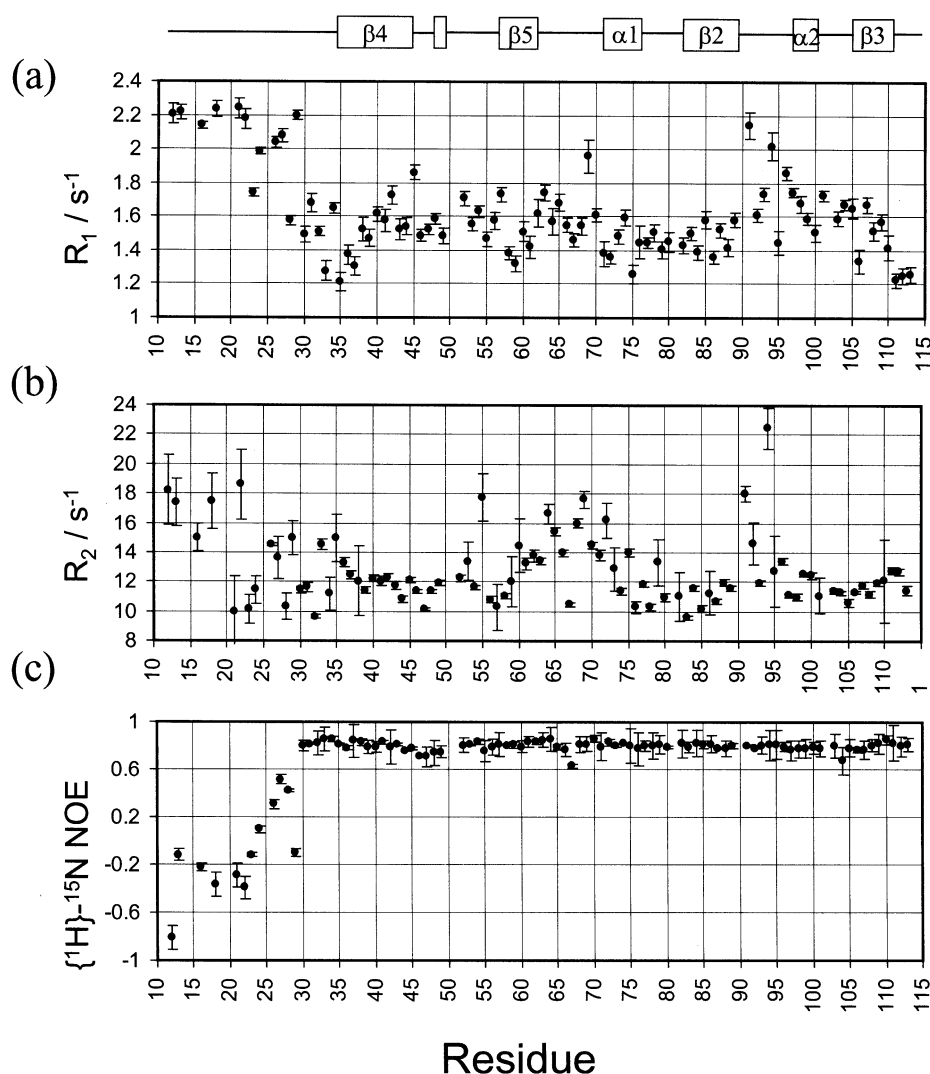
Figure 11. Plots of (a) ^{15}N longitudinal relaxation rate (R_1), (b) ^{15}N transverse relaxation rates (R_2) and (c) {^{1}H}–^{15}N NOE (from top to bottom) as a function of residue number for TF$_{PPIase}$ at 298 K and 600 MHz. Residues for which no results are shown correspond either to proline residues, to unassigned, or to overlapped residues. The location of the β-strands and the α-helices within the structure is sketched above the panels.

<0.65. In this region we find large errors of the R_2 values due to multiexponential decay of the experimental data. Hence, the flexible tail may not adopt a random-coil conformation. On the basis of our studies on TF$_{168-251}$ (see above and Figure 7), this observation supports our postulation, that the N terminus forms a "nascent" β strand interacting with the edge of the β sheet.

The considerable variation of relaxation rates over the entire protein ranging from 1.21 s^{-1} to 2.24 s^{-1} for R_1 and from 9.57 s^{-1} to 22.5 s^{-1} for R_2 indicates that TF$_{PPIase}$ is subjected to significant intramolecular motions on the nanosecond time-scale as well as conformational motion on the microsecond to millisecond time-scale.

Reduced spectral density mapping is a convenient method to characterize the motion of each N–H bond at 0, ω_N, and $0.87\omega_H$ frequency.[55,56] Values obtained for TF$_{PPIase}$ are depicted in Figure 12(a)–(c). In general, the spectral density function $J(\omega)$ of flexible residues decays slowly towards higher values of ω, resulting in an increase of $J(0.87\omega_H)$ (Figure 12(c)) and a decrease of $J(0)$ (Figure 12(a)). On the other hand, exchange broadening gives rise to an increase of $J(0)$. These micro- to millisecond motions, which are most relevant for biological function, have no effect on $J(\omega_N)$ or $J(0.87\omega_H)$. Thus, residues undergoing slow motion can be extracted by analyzing $J(0)$ values (Figure 12(c)).

In the case of anisotropic tumbling, $J(0)$ depends on the dynamics and on the orientation of each N–H vector. Since TF$_{PPIase}$ is expected to tumble anisotropically, as judged from the ratio of the eigenvalues of the inertial tensor (1.00:0.84:0.52), we calculated scaled $J^{eff}(0)$ values that depend on only the dynamics of a given residue.[57] The averaged $J^{eff}(0)$ was determined from rigid residues in secondary structure elements and amounts to 3.08($\pm$0.32) ns (Figure 12(d)). Hence, an average
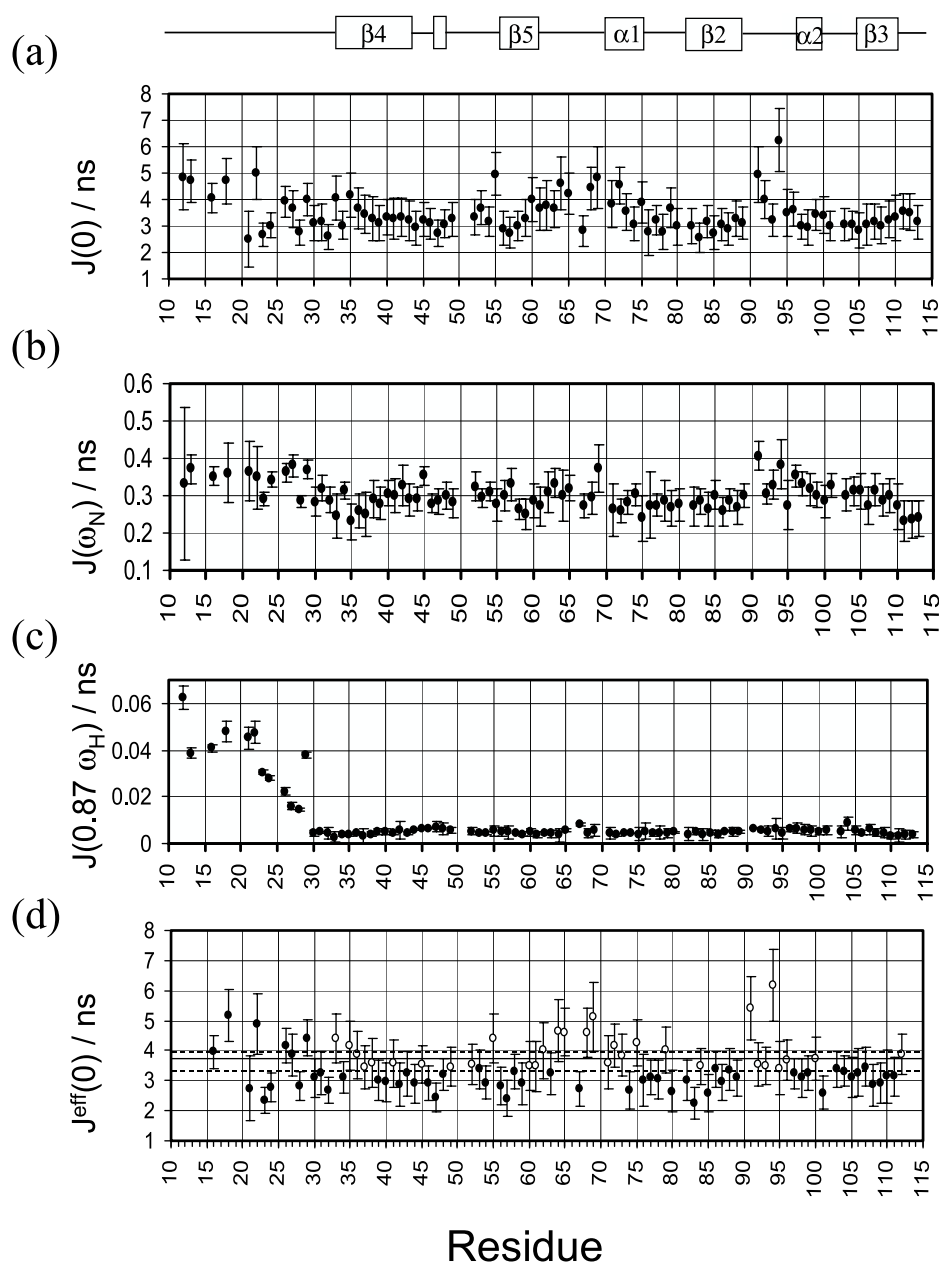
Figure 12. Plots of the reduced spectral density (a) $J(0)$, (b) $J(\omega_N)$, (c) $J(0.87\omega_H)$ and (d) the scaled spectral density $J^{eff}(0)$ as a function of residue number for TF$_{PPIase}$. The location of secondary structure elements within the structure is sketched above the panels. Values for the reduced spectral density $J(0)$, $J(\omega_N)$, $J(0.87\omega_H)$ (a)–(c) were calculated using method 2 from Konradi *et al.*[56]. (d) Values for the scaled spectral density $J^{eff}(0)$ were calculated as described.[57] The average $J^{eff}(0)$ is indicated by a horizontal full line and the standard deviation of $J^{eff}(0)$ by broken lines. For the structured part, values with $J^{eff}(0) > 3.4$ ns indicating significant exchange broadening are marked with open circles.

overall correlation time of $\tau_m^{eff} = 2.5$, $J^{eff}(0) = 7.7(\pm0.7)$ ns can be defined, which is a reasonable value for a monomeric protein of this size. This value cannot be compared to the overall correlation time of FKBP (9.2 ns) directly, because the measurements were carried out at significantly different temperature (303 K) and protein concentration (8.6 mM).[58] The authors attribute the large τ_m value of FKBP to possible solution viscosity effects arising from the high protein concentration.

Considering only the structured part of TF$_{PPIase}$, we define residues with $J^{eff}(0) > 3.4$ ns being sensi-

tive to chemical exchange and/or conformational averaging effects (Figure 12(d)). However, these large $J^{eff}(0)$ values do not provide information regarding the precise time-scale or amplitude of the motion. Figure 5(a) displays a mapping of these residues on our structure. Strikingly, many amino acid residues in the loop region from Ser63 to Gly69 and in the flap region from Ser91 to Lys96 show considerable conformational motion. The TF$_{PPIase}$ 50s-bulge and the tight turn between the strands β4 and β5 exhibit this kind of motion to a smaller extent. Surprisingly, amide groups

that are hydrogen bonded in well-defined secondary structure elements appear to exhibit conformational motions. Notable are the α1-helix, the end of the strand β5 (Thr60, Ile61), the beginning of the strand β4 (Gly33 to Ile38), as well as the residues Val107 and Thr84 from the central part of the β sheet.

The TF$_{PPIase}$ structure can be described as a bent hand with the palm being the β-sheet, the thumb forming the flap region, and the fingers comprising the ends of the β-strands plus helix α1. Using this picture, the conformational motion of TF$_{PPIase}$ describing our relaxation data can be visualized as an opening and closing of this hand. Residues Thr84, Val107, Thr41, and Glu55 (located across all strands of the central β sheet) would act as a hinge. Such breathing motions were observed for FKBP.[58] When all amide protons with chemical exchange line-widths larger than 2 Hz are mapped on the structure of FKBP, the corresponding regions are affected (Figure 5(b)). Thus, from our relaxation data we conclude that TF$_{PPIase}$ and FKBP exert similar motions.

In both proteins, the residues with increased flexibility include the protein–substrate interface discussed above, most notably the loop including helix α1, residues within the 40s bulge in FKBP (50s bulge in TF$_{PPIase}$) and the flap region. It is reasonable to assume that motions within the intermolecular interface are relevant for the binding process. Indeed, the available data on FKBP support this view. In the FK506–FKBP complex, residues within the flap region (residue 82–87) were found to be more rigid than in free FKBP, as indicated by damped internal motions at these sites.[59] It is therefore probable that a picture similar to that of FK506 bound to FKBP emerges when proline-containing peptides are bound to TF$_{PPIase}$. We are currently investigating the effect of the standard substrate peptide Suc-Ala-Ala-Pro-Phe-pNO$_2$ on the dynamics of TF$_{PPIase}$.

Conclusions

The NMR structure of TF$_{PPIase}$ agrees well with previously published structural models that are based on sequence homology with FKBP. TF$_{PPIase}$ adopts a four-stranded β-sheet structure found also in FKBP and other PPIases. The N-terminal β1 strand of FKBP was not structured in TF$_{PPIase}$. However, our data suggest that this N terminus may form a nascent strand by partially adhering to the edge of the central β-sheet. In addition to structural similarity, we observe dynamic similarity of the two proteins. Characteristic differences from the predicted structure were found in those regions that differ in sequence most strongly from that of FKBP, in particular the flap and the 40s bulge regions. These regions may be responsible for substrate recognition and specific interactions with other proteins.

Despite the high degree of conservation within the active site of TF$_{PPIase}$, two distinct structural differences can explain the inability of TF$_{PPIase}$ to bind FK506: (1) a replacement of a non-conserved Val by Phe; and (2) backbone structure variations involving a conserved tyrosine residue. Both effectively narrow the active site, thereby causing steric clashes that prohibit binding of FK506.

Finally, our structure can explain all currently published mutational data on TF. Most of these mutations unsuccessfully attempted to re-establish FK506 binding by designing a more FKBP-like TF$_{PPIase}$. From the structure, it is now evident that this could not be expected, since mutations of the most critical residues that narrow the active site were not undertaken. Our structural data suggest that mutating Phe66 and Tyr93 to less bulky hydrophobic residues may enable FK506 binding.

Materials and Methods

Overexpression and purification of the trigger factor

The PPIase domain TF$_{151–251}$ (denoted TF$_{PPIase}$ in the text) including an N-terminal His-tag (MRGSHHHH-HHGS) was cloned and overexpressed in *E. coli* and purified as described.[20]

The TF$_{PPIase}$ and the deletion mutant TF$_{168–251}$ both devoid of the His$_6$ tag were amplified with the N-terminal *Nco* I-site primers (5′-ggggaagggccatgggc-gaaaagctgg-3′) for TF$_{PPIase}$ and (5′-ggggaaggg*ccatggg*-caaaaaactagctaatggtg-3′) for TF$_{168–251}$ and the C-terminal *Bam* HI-site primer (5′-ggggtttggg*ggatcc*agggtcgac-3′) and cloned into the vector pKM263,[60] an expression vector with an N-terminal cleavable glutathione-S-transferase (GST) fusion protein. The resulting plasmid, pKMTF, was transformed in *E. coli* BL21DEIII pLysS (Novagen). Expression in M9 minimal medium, purification and cleavage of the GST fusion protein were done as described[60] with minor modifications.

NMR spectroscopy

All NMR experiments were recorded at 298 K on Bruker DRX600 and DRX800 spectrometers at 600 and 800 MHz proton resonance frequencies, respectively. For assignment purposes, samples with 2 mM protein concentration were used. The following samples were prepared: (1) U–^{15}N; (2) U–^{13}C/U–^{15}N; (3) unlabeled protein. All spectra were run in 50 mM sodium phosphate buffer (pH 6.5). For the HCCH-total correlated spectroscopy (TOCSY), the 80 ms ^{13}C-NOESY-HMQCs and 80 ms 2D-NOESY, the samples were dissolved in 100% ^{2}H$_2$O. All other spectra were recorded in 90% H$_2$O/10% ^{2}H$_2$O.

The following multidimensional experiments were recorded and evaluated: (a) backbone assignment: HNCO, HNCA, CBCA(CO)NH, HNCACB; (b) side-chain assignment: (H)CC(CO)NH-TOCSY, HCCH-TOCSY, 80 ms ^{15}N-NOESY-HSQC, 60 ms ^{15}N-TOCSY-HSQC, 80 ms ^{13}C-NOESY-HMQC (aliphatic region), 80 ms ^{13}C-NOESY-HMQC (aromatic region); (c) additional spectra for structure elucidation: HNHA, 80 ms 2D-NOESY. NOEs involving aromatic protons were extracted from the latter spectrum. S^{3}E ^{1}H–^{15}N HSQC spectra[61] in partially aligning medium (5% *n*-dodecyl-penta(ethylene glycol):hexanol 0.96:1)[62] were recorded for evaluation of residual dipolar couplings.

All 3D spectra were processed by Bruker xwinnmr1.3 software including linear prediction and apodization by shifted sinebell functions. Backbone and side-chain resonances were assigned using Felix (MSI) and xeasy.[63]

[15]N relaxation data were obtained on a 1.5 mM concentrated (U–[15]N)-labeled TF$_{PPIase}$ sample. Backbone amide {[1]H}–[15]N NOE, [15]N R_1, [15]N R_2 (CPMG) values were measured at 298 K and 600 MHz with conventional pulse sequences.[64] The [15]N R_1 and the [15]N R_2 relaxation decays were sampled at eight different time-points each (T_1 delays = 0.005, 0.079, 0.159, 0.239, 0.359, 0.519, 0.759, and 1.119 seconds; T_2 delays = 0.009, 0.017, 0.034, 0.060, 0.086, 0.112, 0.148, 0.190 seconds) with duplicate spectra for all time-points. All R_1 and R_2 spectra were acquired with 128 × 1024 complex points and with spectral widths of 2.067 × 8.503 kHz in the $t_1 \times t_2$ dimensions. A recycle delay of three seconds and eight transients were applied. For the unsaturated {[1]H}–[15]N NOE measurement, a recycle delay of five seconds was used. This recycle delay was substituted in the presaturated {[1]H}–[15]N NOE experiment with a 0.5 second delay followed by a 4.5 second long series of non-selective 120° [1]H pulses separated by 5 ms delay. The NOE-spectra were recorded in an interleaved manner with 64 transients each.

Distance, dihedral angle and orientation restraints

Evaluation and assignment of NOESY spectra was accomplished with xeasy.[63] NOEs from the ^{15}N-edited 3D-NOESY-HSQC and from the 2D homonuclear NOESY were classified either as very weak, weak, medium, or strong with an upper distance restraint of 5.6, 4.6, 3.0 and 2.9 Å, respectively. NOEs from ^{13}C-edited NOESY-HSQC spectra were classified as strong to medium (4.5 Å) or weak (5 Å), reflecting the reduced sensitivity and resolution of these ^{13}C-edited spectra. In all cases, no lower distance limit was applied.

Hydrogen bonds were introduced for amide protons where the exchange against deuterium was not complete after 20 hours. One additional hydrogen bond (Ala76(NH)–Thr72(O)) emerged from the resulting structures and was introduced at a later stage of the calculation. Hydrogen bonds were defined as double restraint, from the carbonyl oxygen atom to the amide hydrogen and nitrogen atoms, using standard lengths for hydrogen bonds.

$^3J_{HN-H\alpha}$ coupling constants were extracted from a 3D HNHA experiment.[65] In addition to J coupling restraints (see below), dihedral angle restraints for ψ were applied in an iterative way, i.e. after the corresponding amino acid residues began to cluster within the Ramachandran plot. Generally, values of $120(\pm 40)°$ for β-sheet regions and $65(\pm 20)°$ for α-helices were applied. For residues that emerged in the positive ψ range, a value of $60(\pm 40)°$ was applied.

Dipolar splittings were evaluated from the resonance positions derived from two spin-state selective, ω_1-coupled ^{1}H–^{15}N HSQC spectra.[61] Splittings were subsequently converted to intervector projection restraints using the DipoCoup program.[33]

Structure calculation and analysis

Structures were calculated using the CHARMM force field with the CNS program package.[31] CNS was extended to incorporate residual dipolar coupling restraints[30] (program files available online from ftp://

ftp.EMBL-Heidelberg.DE/nmr/nilges/arianew/cns_1.0_10042000). A four-stage molecular dynamics protocol was used; (a) 500 steps/7.5 ps torsion angle molecular dynamics at 10,000 K; (b) 1000 steps/15 ps cooling to 0 K; (c) 5000 steps/25 ps Cartesian molecular dynamics cooling from 2000 K to 0 K; (d) extensive minimization. Prochiral valine and leucine methyl groups were treated with floating chirality.

The resulting NMR structures were evaluated with MOLMOL[66] and PROCHECK.[32] Figures were prepared and electrostatic surface potentials were calculated with MOLMOL.

Structural data for comparison with the FKBP structure were taken from PDB entries 1FKF for the FKBP–FK506 complex,[38,40] 1D6O for uncomplexed FKBP and 1D7H for the FKBP–DMSO complex,[37] 1PIN for human Pin1[42] and 1EQ3 for parvulin.[5]

Relaxation analysis

Relaxation NMR spectra were processed and analyzed with Felix 2000 software (Biosym Technologies, Inc.). Backbone amide [15]N R_1 and R_2 relaxation rates were determined by fitting of peak heights as functions of relaxation decay times to single-exponential decay functions. Steady-state NOE values were calculated from the ratios of the peak intensities with and without proton saturation.[54] Uncertainties in measurements of peak height were estimated from base-line noise.[67] Spectral densities were calculated at $\omega = 0$, ω_N, and $0.87\omega_H$ from R_1, R_2, and {[1]H}–[15]N NOE data using the approximation $J(0) = \text{const}$ or $J(\omega) \propto 1/\omega^2$ for $\omega = \omega_H \pm \omega_N$.[56] Since the eigenvalues of the inertial tensor are in the ratio of 1.00:0.84:0.52 for the best calculated structure, TF$_{PPIase}$ is expected to tumble anisotropically. As a consequence, $J(0)$ depends on the orientation of the individual N–H bonds. Therefore, $J(0)$ was scaled up to residue-independent $J^{eff}(0)$ values using the procedure described.[57] Based on our structure, the anisotropy factor σ was calculated as $\sigma = D_{\parallel}/D_{\perp} = 1.6$ with the shape of TF$_{PPIase}$ approximated to a symmetrical ellipsoid. The angle α between the N–H bond vector and the long axis was extracted from the 3D structure. This led to scaling factors between 0.86 and 1.10. Anisotropic effects for $J^{eff}(0)$ can be neglected in most real cases.[57] $J^{eff}(0)$ then depends on only the dynamics: internal motions give rise to lower than the average $J^{eff}(0)$, whereas exchange broadening causes higher values. The average of $J^{eff}(0)$ values was taken from 19 residues in secondary structure elements that show little flexibility (residues 39, 40, 42–44, 47, 48, 85–89, 97–99, 103–106). It amounts to $3.1(\pm 0.3)$ ns.

Binding studies

TF$_{PPIase}$–FK506 binding studies were conducted by recording saturation transfer difference (STD) spectra[49] and by monitoring chemical shift changes in ^{1}H–^{15}N HSQC spectra. Spectra with the same amount of DMSO were used as a reference. FK506 (Calbiochem, San Diego) was dissolved in DMSO and added as stock solution to yield a 10% DMSO/90% buffer solution. Under these conditions, ca 0.5 mM FK506 is soluble as judged from relative signal intensities with a standard of known concentration (0.2 mM 3,3,3-trimethylsilyl-propionate (TSP)). For STD spectra, a tenfold excess of FK506 over the protein was used. To determine affinities, ligands (DMSO or peptide) were added stepwise. In STD spectra, saturation was achieved by a series of equally

spaced 50 ms Gaussian-shaped pulses, with a peak amplitude of 10 Hz, 10 ms delay between the pulses, and a total saturation time of about two seconds.

Data Bank accession codes

The structures shown in Figure 4 have been submitted to the RCSB Protein Data Bank, with ID code 1HXV. Backbone and C$^\alpha$ resonances were assigned using a combination of 3D HNCACB and 3D CBCA(CO)NH spectra. For the structured region of TF$_{PPIase}$ all residues, except Ala50, give rise to distinct amide cross-peaks. The assignment and the extent of assigned resonances have been submitted to the BioMagResBank with accession number 4953.

References

1. Göthel, S. F. & Marahiel, M. A. (1999). Peptidyl-prolyl *cis–trans* isomerases, a superfamily of ubiquitous folding catalysts. *Cell. Mol. Life Sci.* **55**, 423–436.
2. Drakenberg, T. & Forsén, S. (1970). The barrier to internal rotation in amides. I. Formamide. *J. Phys. Chem.* **74**, 1–7.
3. Netzer, W. J. & Hartl, F. U. (1998). Protein folding in the cytosol: chaperonin-dependent and -independent mechanisms. *Trends Biochem. Sci.* **23**, 68–73.
4. Hartl, F. U. (1996). Molecular chaperones in cellular protein folding. *Nature*, **381**, 68–73.
5. Sekerina, E., Rahfeld, J. U., Müller, J., Fanghänel, J., Rascher, C., Fischer, G. & Bayer, P. (2000). NMR solution structure of *h*Par14 reveals similarity to the peptidyl prolyl *cis/trans* isomerase domain of the mitotic regulator *h*Pin1 but indicates a different functionality of the protein. *J. Mol. Biol.* **301**, 1003–1017.
6. Crooke, E. & Wickner, W. (1987). Trigger factor: a soluble protein that folds pro-OmpA into a membrane-assembly-competent form. *Proc. Natl Acad. Sci. USA*, **84**, 5216–5220.
7. Crooke, E., Guthrie, B., Lecker, S., Lill, R. & Wickner, W. (1988). ProOmpA is stabilized for membrane translocation by either purified *E. coli* trigger factor or canine signal recognition particle. *Cell*, **54**, 1003–1011.
8. Stoller, G., Rücknagel, K. P., Nierhaus, K. H., Schmid, F. X. & Rahfeld, J. U. (1995). A ribosome-associated peptidyl-prolyl *cis/trans* isomerase identified as the trigger factor. *EMBO J.* **14**, 4939–4948.
9. Hesterkamp, T., Hauser, S., Lutcke, H. & Bukau, B. (1996). *Escherichia coli* trigger factor is a prolyl isomerase that associates with nascent polypeptide chain. *Proc. Natl Acad. Sci. USA*, **93**, 4437–4441.
10. Scholz, C., Stoller, G., Zarndt, T., Fischer, G. & Schmid, F. X. (1997). Cooperation of enzymatic and chaperone functions of trigger factor in the catalysis of protein folding. *EMBO J.* **16**, 54–58.
11. Hesterkamp, T., Deuerling, E. & Bukau, B. (1997). The amino-terminal 118 amino acids of *Escherichia coli* trigger factor constitute a domain that is necessary and sufficient for binding to ribosomes. *J. Biol. Chem.* **272**, 21865–21871.
12. Zarnt, T., Tradler, T., Stoller, G., Scholz, C., Schmid, F. X. & Fischer, G. (1997). Modular structure of the trigger factor required for high activity in protein folding. *J. Mol. Biol.* **271**, 827–837.
13. Scholz, C., Mücke, M., Rape, M., Pecht, A., Pahl, A., Bang, H. & Schmid, F. X. (1998). Recognition of protein substrates by the prolyl isomerase trigger factor is independent of proline residues. *J. Mol. Biol.* **277**, 723–732.
14. Nishihara, K., Kanemori, M., Yanagaki, H. & Yura, T. (2000). Overexpression of trigger factor prevents aggregation of recombinant proteins in *Escherichia coli*. *Appl. Environ. Microbiol.* **66**, 884–889.
15. Deuerling, E., Schulze-Specking, A., Tomoyasu, T., Mogk, A. & Bukau, B. (1999). Trigger factor and DnaK cooperate in folding of newly synthesized proteins. *Nature*, **400**, 693–696.
16. Teter, S. A., Houry, W. A., Ang, D., Tradler, T., Rockabrand, D., Fischer, G. *et al.* (1999). Polypeptide flux through bacterial Hsp70: DnaK cooperates with trigger factor in chaperoning nascent chains. *Cell*, **97**, 755–765.
17. Kandror, O., Sherman, M., Moerschell, R. & Goldberg, A. L. (1997). Trigger factor associates with GroEL *in vivo* and promotes its binding to certain polypeptides. *J. Biol. Chem.* **272**, 1730–1734.
18. Kandror, O. & Goldberg, A. L. (1997). Trigger factor is induced upon cold shock and enhances viability of *Escherichia coli* at low temperatures. *Proc. Natl Acad. Sci. USA*, **94**, 4978–4981.
19. Fraser, C. M., Gocayne, J. D., White, O., Adams, M. D., Clayton, R. A., Fleischmann, R. D. *et al.* (1995). The minimal gene complement of *Mycoplasma genitalium*. *Science*, **270**, 397–403.
20. Bang, H., Pecht, A., Raddatz, G., Scio, T., Solbach, W., Brune, K. & Pahl, A. (2000). Prolyl isomerases in a minimal cell. Catalysis of protein folding by trigger factor from *Mycoplasma genitalium*. *Eur. J. Biochem.* **267**, 3270–3280.
21. Hesterkamp, T. & Bukau, B. (1996). Identification of the prolyl isomerase domain of *Escherichia coli* trigger factor. *FEBS Letters*, **385**, 67–71.
22. Stoller, G., Tradler, T., Rücknagel, K. P., Rahfeld, J. U. & Fischer, G. (1996). An 11.8 kDa proteolytic fragment of the *E. coli* trigger factor represents the domain carrying the peptidyl-prolyl *cis/trans* isomerase activity. *FEBS Letters*, **384**, 117–122.
23. Göthel, S. F., Schmid, R., Wipat, A., Carter, N. M., Emmerson, P. T., Harwood, C. R. & Marahiel, M. A. (1997). An internal FK506-binding domain is the catalytic core of the prolyl isomerase activity associated with the *Bacillus subtilis* trigger factor. *Eur. J. Biochem.* **244**, 59–65.
24. Callebaut, I. & Mornon, J.-P. (1995). Trigger factor, one of the *Escherichia coli* chaperone proteins, is an original member of the FKBP family. *FEBS Letters*, **374**, 211–215.
25. Wittekind, M. & Müller, L. (1993). HNCACB, a high-sensitivity 3D NMR experiment to correlate amide-proton and nitrogen resonances with the alpha- and beta-carbon resonances in proteins. *J. Magn. Reson. ser. B*, **101**, 201–205.

26. Grzesiek, S. & Bax, A. (1992). Correlating backbone amide and side-chain resonances in larger proteins by multiple relayed triple resonance NMR. *J. Am. Chem. Soc.* **114**, 6291–6293.

27. Parac, T. N., Vogtherr, M., Maurer, M., Pahl, A., Rüterjans, H., Griesinger, C. & Fiebig, K. (2001). Assignment of the ^{1}H, ^{13}C and ^{15}N resonances of the PPIase domain of the trigger factor from *Mycoplasma genitalium*. *J. Biomol. NMR*, **20**, 193–194.

28. Fiebig, K., Schwalbe, H., Buck, M., Smith, L. J. & Dobson, C. M. (1996). Towards a description of the conformations of denatured states of proteins. Comparison of a random coil model with NMR measurements. *J. Phys. Chem.* **100**, 2661–2666.

29. Schwalbe, H., Fiebig, K. M., Buck, M., Jones, J. A., Grimshaw, S. B., Spencer, A. *et al.* (1997). Structural and dynamical properties of a denatured protein. Heteronuclear 3D NMR experiments and theoretical simulations of lysozyme in 8 M urea. *Biochemistry*, **36**, 8977–8991.

30. Meiler, J., Blomberg, N., Nilges, M. & Griesinger, C. (2000). A new approach for applying residual dipolar couplings as restraints in structure elucidation. *J. Biomol. NMR*, **16**, 245–252.

31. Brünger, A. T., Adams, P. D., Clore, G. M., DeLano, W. L., Gros, P., Grosse-Kunstleve, R. W. *et al.* (1998). Crystallography & NMR system: a new software suite for macromolecular structure determination. *Acta Crystallog. sect. D*, **54**, 905–921.

32. Laskowski, R. A., MacArthur, M. W., Moss, D. S. & Thornton, J. M. (1993). PROCHECK: a program to check the stereochemical quality of protein structures. *J. Appl. Crystallog.* **26**, 283–291.

33. Meiler, J., Peti, W. & Griesinger, C. (2000). DipoCoup: a versatile program for 3D-structure homology comparison based on residual dipolar couplings and pseudocontact shifts. *J. Biomol. NMR*, **17**, 283–294.

34. Cornilescu, G., Marquardt, J. L., Ottiger, M. & Bax, A. (1998). Validation of protein structure from anisotropic carbonyl chemical shifts in a dilute liquid crystalline phase. *J. Am. Chem. Soc.* **120**, 6836–6837.

35. Pervushin, K. V., Riek, R., Wider, G. & Wüthrich, K. (1997). Attenuated T_2 relaxation by mutual cancellation of dipole–dipole coupling and chemical shift anisotropy indicates an avenue to NMR structures of very large biological macromolecules in solution. *Proc. Natl Acad. Sci. USA*, **94**, 12366–12371.

36. Crowley, P., Ubbink, M. & Otting, G. (2000). Φ angle restraints in protein backbones from dipole–dipole cross-correlation between ^{1}H^N–^{15}N and ^{1}H^N–^{1}H$^\alpha$ vectors. *J. Am. Chem. Soc.* **122**, 2968–2969.

37. Burkhard, P., Taylor, P. & Walkinshaw, M. D. (2000). X-ray structures of small ligand–FKBP complexes provide an estimate for hydrophobic interaction energies. *J. Mol. Biol.* **295**, 953–962.

38. Van Duyne, G. D., Standaert, R. F., Karplus, P. A., Schreiber, S. L. & Clardy, J. (1991). Atomic structure of FKBP-FK506, an immunophilin–immunosuppressant complex. *Science*, **252**, 839–842.

39. Van Duyne, G. D., Standaert, R. F., Schreiber, S. L. & Clardy, J. (1991). Atomic structure of the rapamycin human immunophilin FKBP-12 complex. *J. Am. Chem. Soc.* **113**, 7433.

40. Van Duyne, G. D., Standaert, R. F., Karplus, P. A., Schreiber, S. L. & Clardy, J. (1993). Atomic structures of the human immunophilin FKBP-12 complexes with FK506 and rapamycin. *J. Mol. Biol.* **229**, 105–124.

41. Richardson, J. S. (1977). β-Sheet topology and the relatedness of proteins. *Nature*, **268**, 495–500.

42. Ranganathan, R., Lu, K. P., Hunter, T. & Noel, J. P. (1997). Structural and functional analysis of the mitotic rotamase Pin1 suggests substrate recognition is phosphorylation dependent. *Cell*, **89**, 875–886.

43. Patzelt, H., Rüdiger, S., Brehmer, D., Kramer, G., Vorderwülbecke, S., Schaffitzel, E. *et al.* (2001). Binding specificity of *Escherichia coli* trigger factor. *Proc. Natl Sci. USA*, **98**, 14244–14249.

44. Orozco, M., Tirado-Rives, J. & Jorgensen, W. L. (1993). Mechanism for the rotamase activity of FK506 binding protein from molecular dynamics simulations. *Biochemistry*, **32**, 12864–12874.

45. Fischer, S., Michnick, S. & Karplus, M. (1993). A mechanism for rotamase catalysis by the FK506 binding protein (FKBP). *Biochemistry*, **32**, 13830–13837.

46. Tradler, T., Stoller, G., Rücknagel, K. P., Schierhorn, A., Rahfeld, J. U. & Fischer, G. (1997). Comparative mutational analysis of peptidyl *cis/trans* isomerases: active sites of *Escherichia coli* trigger factor and human FKBP12. *FEBS Letters*, **407**, 184–190.

47. Galat, A. (2000). Sequence diversification of the FK506-binding proteins in several different genomes. *Eur. J. Biochem.* **267**, 4945–4959.

48. Griffith, J. P., Kim, J. L., Kim, E. E., Sintchak, M. D., Thomson, J. A., Fitzgibbon, M. J. *et al.* (1995). X-ray structure of calcineurin inhibited by the immunophilin–immunosuppressant FKBP12–FK506 complex. *Cell*, **82**, 507–522.

49. Mayer, M. & Meyer, B. (1999). Characterization of ligand binding by saturation transfer difference NMR spectroscopy. *Angew. Chem. Int. Ed. Engl.* **38**, 1784–1788.

50. Kofron, J. L., Kuzmic, P., Kishore, V., Colon-Bonilla, E. & Rich, D. H. (1991). Determination of kinetic constants for peptidyl prolyl *cis–trans* isomerases by an improved spectrophotometric assay. *Biochemistry*, **30**, 6127–6134.

51. Dalvit, C., Floersheim, P., Zurini, M. & Widmer, A. (1999). Use of organic solvents and small molecules for locating binding sites on proteins in solution. *J. Biomol. NMR*, **14**, 23–32.

52. Schiene, C., Reimer, U., Schutkowski, M. & Fischer, G. (1998). Mapping the stereospecificity of peptidyl prolyl *cis/trans* isomerases. *FEBS Letters*, **432**, 202–206.

53. Harrison, R. K. & Stein, R. L. (1990). Substrate specificities of the peptidyl prolyl *cis–trans* isomerase activities of cyclophilin and FK-506 binding protein: evidence for the existence of a family of distinct enzymes. *Biochemistry*, **29**, 1813–3816.

54. Grzesiek, S. & Bax, A. (1993). The importance of not saturating H_2O in protein NMR. Application to sensitivity enhancement and NOE measurements. *J. Am. Chem. Soc.* **115**, 12593–12594.

55. Peng, J. W. & Wagner, G. (1995). Frequency spectrum of NH bonds in Eglin c from spectral density mapping at multiple fields. *Biochemistry*, **34**, 16733–16752.

56. Farrow, N. A., Zhang, O., Szabo, A., Torchia, D. A. & Kay, L. E. (1995). Spectral density function mapping using ^{15}N relaxation data exclusively. *J. Biomol. NMR*, **6**, 153–162.

57. Renner, C., Baumgartner, R., Noegel, A. A. & Holak, T. A. (1998). Backbone dynamics of the CDK inhibitor p19[INK4d] studied by ^{15}N NMR relaxation experiments at two field strengths. *J. Mol. Biol.* **283**, 221–229.

58. Cheng, J.-W., Lepre, C. A., Chambers, S. P., Fulghum, J. R., Thomson, J. A. & Moore, J. M. (1993). ^{15}N NMR relaxation studies of the FK-506 binding protein: backbone dynamics of the uncomplexed receptor. *Biochemistry*, **32**, 9000–9010.

59. Cheng, J.-W., Lepre, C. A. & Moore, J. M. (1994). ^{15}N NMR relaxation studies of the FK506 binding protein: dynamic effects of ligand binding and implications for calcineurin recognition. *Biochemistry*, **33**, 4093–4100.

60. Melcher, K. (2000). A modular set of prokaryotic and eukaryotic expression vectors. *Anal. Biochem.* **277**, 109–120.

61. Meissner, A., Duus, J.Ø. & Sørensen, O. W. (1997). Integration of spin-state-selective excitation into 2D NMR correlation experiments with heteronuclear ZQ/2Q ϕ rotations for $^1J_{XH}$. *J. Biomol. NMR*, **10**, 89–94.

62. Rückert, M. & Otting, G. (2000). Alignment of biological macromolecules in novel nonionic liquid crystalline media for NMR experiments. *J. Am. Chem. Soc.* **122**, 7793–7797.

63. Bartels, C., Xia, T.-H., Billeter, M., Güntert, P. & Wüthrich, K. (1995). The program XEASY for computer-supported NMR spectral analysis of biological macromolecules. *J. Biomol. NMR*, **5**, 1–10.

64. Kay, L. E., Torchia, D. A. & Bax, A. (1989). Backbone dynamics of proteins as studied by ^{15}N inverse detected heteronuclear NMR spectroscopy: application to staphylococcal nuclease. *Biochemistry*, **28**, 8972–8979.

65. Vuister, G. W. & Bax, A. (1993). Quantitavie J correlation: a new approach for measuring homonuclear three bond $J(H_NH_\alpha)$ coupling constants in ^{15}N-enriched proteins. *J. Am. Chem. Soc.* **115**, 7772–7777.

66. Konradi, R., Billeter, M. & Wüthrich, K. (1996). MOLMOL: a program for display and analysis of macromolecular structures. *J. Mol. Graph.* **14**, 51–55.

67. Nicholson, L. K., Kay, L. E., Baldisseri, D. M., Arango, J., Young, P. E., Bax, A. & Torchia, D. A. (1992). Dynamics of methyl groups in proteins as studied by proton-detected ^{13}C NMR spectroscopy. Application to the leucine residues of staphylococcal nuclease. *Biochemistry*, **31**, 5253–5263.

Edited by J. Karn

IDE▲L®

http://www.academicpress.com/jmb

Supplementary Material comprising two Figures of the ^1H–^{15}N HSQC spectra of TF$_{PPIase}$ and of the deletion mutants, and one Figure showing the electric surface potential and van der Waals surface of TF$_{PPIase}$ is available at IDEAL.